ISSN 0006-2979, Biochemistry (Moscow), 2019, Vol. 84, Suppl. 1, pp. S32-S50. © Pleiades Publishing, Ltd., 2019.
Russian Text © M. M. Karasev, O. V. Stepanenko, K. A. Rumyantsev, K. K. Turoverov, V. V. Verkhusha, 2019, published in Uspekhi Biologicheskoi Khimii, 2019, Vol. 59, pp. 67-102.

REVIEW

Near-Infrared Fluorescent Proteins and Their Applications

M. M. Karasev[1,2,a], O. V. Stepanenko[1,b], K. A. Rumyantsev[1,3,4,c], K. K. Turoverov[1,5,d], and V. V. Verkhusha[2,3,e]*

[1]*Institute of Cytology, Russian Academy of Sciences, 194064 St. Petersburg, Russia*
[2]*Medicum, University of Helsinki, 00290 Helsinki, Finland*
[3]*Albert Einstein College of Medicine, Bronx, 10461 NY, USA*
[4]*Loginov Moscow Clinical Scientific Center, 111123 Moscow, Russia*
[5]*Peter the Great St. Petersburg Polytechnic University, 195251 St. Petersburg, Russia*
[a]*e-mail: maksim.karasev@helsinki.fi*
[b]*e-mail: lvs@incras.ru*
[c]*e-mail: k.rumyantsev@mknc.ru*
[d]*e-mail: kkt@incras.ru*
[e]*e-mail: vladislav.verkhusha@einstein.yu.edu*

Received August 6, 2018
Revised August 22, 2018
Accepted August 22, 2018

Abstract—High transparency, low light-scattering, and low autofluorescence of mammalian tissues in the near-infrared (NIR) spectral range (~650-900 nm) open a possibility for *in vivo* imaging of biological processes at the micro- and macroscales to address basic and applied problems in biology and biomedicine. Recently, probes that absorb and fluoresce in the NIR optical range have been engineered using bacterial phytochromes – natural NIR light-absorbing photoreceptors that regulate metabolism in bacteria. Since the chromophore in all these proteins is biliverdin, a natural product of heme catabolism in mammalian cells, they can be used as genetically encoded fluorescent probes, similarly to GFP-like fluorescent proteins. In this review, we discuss photophysical and biochemical properties of NIR fluorescent proteins, reporters, and biosensors and analyze their characteristics required for expression of these molecules in mammalian cells. Structural features and molecular engineering of NIR fluorescent probes are discussed. Applications of NIR fluorescent proteins and biosensors for studies of molecular processes in cells, as well as for tissue and organ visualization in whole-body imaging *in vivo*, are described. We specifically focus on the use of NIR fluorescent probes in advanced imaging technologies that combine fluorescence and bioluminescence methods with photoacoustic tomography.

DOI: 10.1134/S0006297919140037

Keywords: fluorescent proteins, biomarkers, bacterial phytochromes, *in vivo* visualization, fluorescence, bioluminescence, biosensors

Introduction of novel methods of deep three-dimensional visualization of tissues, organs, and entire organism has attracted a considerable attention to the development of bright and high-contrast probes. Mammalian tissues display the highest transparency in the so-called near infra-red (NIR) transparency window (~650-900 nm) (Fig. 1a) [1, 2]. Light absorption by hemoglobin, water, lipids, and melanin is at the minimal level in the NIR region of the spectrum. Hence, the NIR light demonstrates higher penetration ability in comparison with the visible light (Fig. 1b). Moreover, autofluorescence of biological tissues and light scattering in them are significantly lower in the NIR spectral region than in the visible one. This explains considerable interest in the development of probes operating in the NIR region of the spectrum.

Abbreviations: BiFC, bimolecular fluorescence complementation; BiPC, bimolecular photoacoustic complementation; BphP, bacterial phytochrome; BV, biliverdin IXα; CBD, chromophore-binding domain; FMT, fluorescence molecular tomography; FP, fluorescent protein; FRET, Förster resonance energy transfer; HO, heme oxygenase; MSOT, multi-spectral optoacoustic tomography; NIR, near-infrared; OM, output module; PA, photoacoustic effect; PCB, phycocyanobilin; PCM, photosensory core module; PET, positron-emission tomography; PPI, protein–protein interactions; SIM, structured illumination microscopy; siRNA, small interfering RNA; TD, time-domain analysis; XCT, X-ray computed tomography.

* To whom correspondence should be addressed.

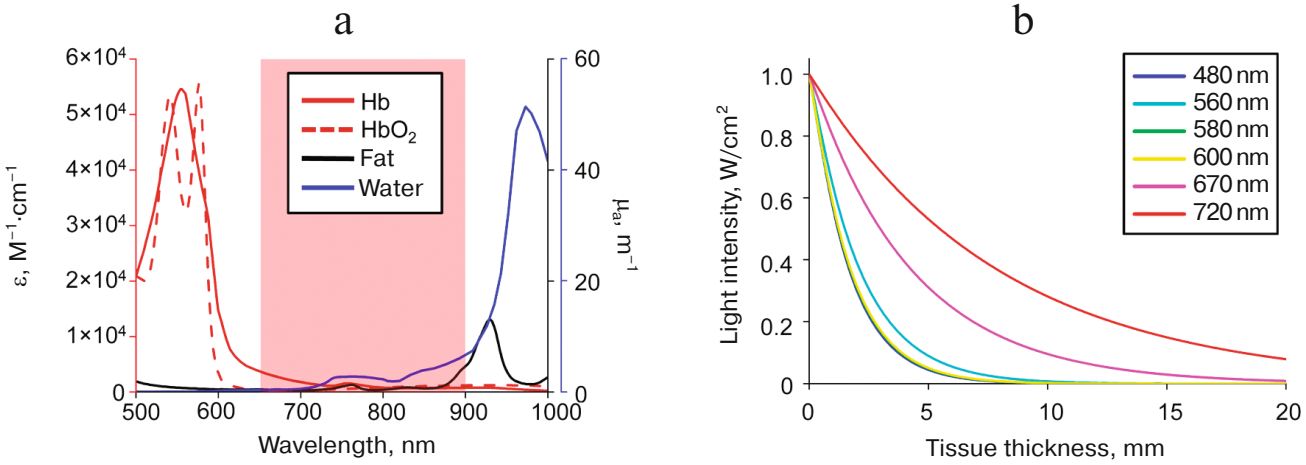

Fig. 1. Light penetration in biological tissues: a) dependence of molar extinction coefficient ε for oxyhemoglobin (HbO_2) and deoxyhemoglobin (Hb) (https://omlc.org/spectra/hemoglobin/summary.html) and light absorption coefficients μ_a for mammalian fat [123] and water [124, 125] on the light wavelength; NIR transparency window for mammalian tissues is marked with a semi-transparent red rectangle; b) attenuation of light of different wavelength in the mammalian muscle tissue (adapted from [100] with permission from Nature Publishing Group, Creative Commons Attribution 4.0 international public license).

Various exogenous NIR fluorescent dyes have been synthesized that could be used for deep *in vivo* visualization technologies. Due to the non-specific interactions of these dyes with proteins in biological tissues, they have to be used in high concentrations to produce contrast images. Targeted delivery of these dyes to specific tissues or organs involves their modification with functional groups (chemical groups, peptides, proteins) and is complicated by the necessity to consider the pharmacokinetic properties of the obtained compounds. This considerably limits the application of synthetic dyes for organ and tissue labeling [3]. A the same time, expression of genetically encoded fluorescent proteins (FPs) can be specifically induced in cells of a certain type, while their endogenous synthesis allows extended non-invasive visualization of molecular processes in an organism without repeated dye administration [4-6].

So far, the attempts to produce sufficiently bright fluorescent biomarkers on the basis of GFP-like proteins with absorption and fluorescence in the NIR range have been unsuccessful. A number of GFP-like proteins, such as TagRFP675 [7], mNeptune681, and mNeptune684 [8], fluoresce in the NIR range due to the large Stokes shift between the absorption and fluorescence spectra. However, the absorption spectra of these biomarkers are still in the far-red region (maximum at ⩽611 nm). The absorption maximum of TagRFP657 [9] is shifted towards the long-wavelength region of the spectrum (611 nm); however, this biomarker has a relatively low molecular brightness typical for the far-red GFP-like proteins.

At present, the most often used compounds for the development of NIR FPs are complexes of bacterial phytochromes (BphPs) containing biliverdin IXα (BV) as a natural prosthetic group with the absorption spectra in the NIR region [10]. Tens of NIR FPs have been generated in the recent decade as a result of BphP engineering. The first NIR FPs displayed a number of drawbacks, which hindered their use as biomarkers including dimeric organization, relatively low fluorescence brightness in mammalian cells, and necessity to use exogenous BV cofactor. Molecular evolution of the NIR FPs directed at solving these problems resulted in the development of bright monomeric spectrally different NIR FPs. Compared to far-red GFP-like proteins, NIR FPs are more suitable to be used as *in vivo* biomarkers [11-13].

NIR FLUORESCENT PROTEINS BASED ON BACTERIAL PHYTOCHROMES

Dimeric NIR FPs. Development of the mutant protein PR-1 with the fluorescence spectrum maximum at 672 nm on the basis of cyanobacterial phytochrome Cph1 can be considered as the first successful example of phytochrome-derived NIR FP [14]. However, because Cph1 chromophore is phycocyanobilin (PCB), application of PR-1 as a biomarker in animal cells was limited by the requirement for either addition of exogenous PCB or its synthesis in the cells. This is the reason why BphP with BV as a chromophore has been used as a template for the development of biomarkers thereafter [15]. BV is formed as a product of heme degradation by heme oxygenase (HO) and is ubiquitous in cells of eukaryotic organisms, including mammals, fish, and insects. This property makes it possible to use BphP-based proteins as geneti-

Photophysical properties of NIR FPs

NIR FP	Natural template	Absorption maximum, nm	Fluorescence maximum, nm	Molar extinction coefficient (EC), $M^{-1}\cdot cm^{-1}$	Fluorescence quantum yield (QY), %	Molecular brightness* vs. iRFP713, %	Effective brightness† vs. iRFP713, %	Reference
Dimeric NIR FPs								
IFP1.4	*Dr*BphP	684	708	92,000	7.7	114	8	[13]
IFP2.0	*Dr*BphP	690	711	98,000	8.1	80	7.9	[17]
smURFP	APC	642	670	180,000	18	551	2‡	[20]
BDFP1.1	ApcF2	682	707	68,700	5.9	42	6	[22]
iRFP682	*Rp*BphP2	663	682	90,000	11.1	162	105	[12]
iRFP713 (iRFP)	*Rp*BphP2	690	713	98,000	6.3	100	100	[11]
iRFP720	*Rp*BphP2	702	720	96,000	6.0	93	110	[12]
iRFP670	*Rp*BphP6	643	670	114,000	12.2	225	119	[12]
iRFP702	*Rp*BphP6	673	702	93,000	8.2	124	61	[12]
PAiRFP1	*At*BphP2	693#	717	67,100	4.8	64	25	[23]
PAiRFP2	*At*BphP2	693#	719	63,600	4.7	60	25	[23]
Monomeric NIR FPs								
Wi-Phy	*Dr*BphP	700	722	118,000	6.3	n.d.	n.d.	[18]
mIFP	*Br*BphP	683	704	82,000	8.4	74	14	[24]
iBlueberry	*Br*BphP	644	667	38,000	6.9	42	n.d.	[25]
BDFP1.5	ApcF2	688	711	74,000	5.0	38	2	[22]
GAF-FP	*Rp*BphP1	635	670	49,800	7.3	59	2	[26]
BphP1-FP	*Rp*BphP1	640	669	60,000	13	126	n.d.	[27]
miRFP670	*Rp*BphP1	642	670	87,400	14	198	72	[29]
miRFP670-2	*Rp*BphP6	643	670	103,000	13.6	226	72	[28]
miRFP682	*Rp*BphP2	663	682	91,000	11.2	165	117	[28]
miRFP702	*Rp*BphP6	673	702	88,000	8.1	115	37	[28]
miRFP703	*Rp*BphP1	674	703	90,900	8.6	127	37	[29]
miRFP709	*Rp*BphP1	683	709	78,400	5.4	69	30	[29]
miRFP713	*Rp*BphP2	690	713	99,000	7.0	111	109	[28]
miRFP720	*Rp*BphP2	702	720	98,000	6.1	97	116	[30]

Note: n.d., not determined.

* Brightness measured for purified protein *in vitro*.

† Brightness upon expression in mammalian cells.

Data for the protein in photoactivated state.

‡ Measured 48 h after transfection without adding of exogenous BV [21].

cally encoded biomarkers (similar to GFP-like proteins) for visualization of cellular processes, because they do not require the use of cofactors or coexpression of auxiliary enzymes [16].

The first NIR FP based on the bacterial phytochrome from *Deinococcus radiodurans* (*Dr*BphP) was developed in the laboratory of Roger Tsien, a pioneer in the fast-developing science of genetically encoded protein-based fluorescent biomarkers, whose contribution to science has been acknowledged by the Nobel Prize in Chemistry for 2008 and whose works have provided the basis for unique technological advancements in molecular and cellular biology. The development of NIR FPs was based on the evolution of the *Dr*BphP chromophore-binding domain (CBD) consisting of the PAS and GAF domains and sufficient for the interaction with the chromophore. Molecular engineering of *Dr*CBD included saturation mutagenesis at positions determined based on the protein structure data, DNA shuffling, and several cycles of directed evolution and resulted in the generation of the bright and stable IFP1.4 biomarker with the fluorescence spectrum maximum at 708 nm [13]. Generation of other NIR FPs revealed that IFP1.4 exhibited far from optimal photophysical characteristics (low level of molecular brightness, low affinity and specificity of BV binding; see table). Nevertheless, *in vivo* application of

IFP1.4 confirmed the advantage of NIR FPs over the red fluorescent proteins (e.g., mKate) owing to significantly less absorption of the excitation and emission light by animal tissues in the NIR spectral range.

Through DNA shuffling of IFP1.4 and IFP1.2 sequences with subsequent library selection (see Fig. 2) the biomarker IFP2.0 was obtained, which exhibits higher molecular brightness comparing to its parental FPs [17]. IFP2.0 was used for labeling neurons in *Drosophila* larvae and glioblastoma cells in mice. However, because of the low affinity toward BV that is inherent to all proteins of the IFP series, this chromophore must be administered exogenously or co-expressed with HO, which has limited wide application of IFP for tissue and organ visualization *in vivo*.

The Wi-Phy and Wi-Phy2 proteins were produced by engineering of *Dr*BphP [18, 19], however, their properties have not been characterized in cell culture or *in vivo*. The three-dimensional structure of these proteins was elucidated by the X-ray diffraction method, and the conformation of the chromophore and amino acids in its immediate vicinity was analyzed, which contributed to the understanding of photophysical mechanisms of NIR fluorescence of the BphP-based markers.

Almost at the same time, a series of spectrally different NIR FPs was produced based on the bacterial phytochromes *Rp*BphP2 and *Rp*BphP6 from *Rhodopseudomonas palustris*. The fluorescence maxima of these NIR FPs termed iRFPs (table) are in the range from 670 to 720 nm [11, 12]. The first protein of this series – iRFP713 (initially called iRFP) [11] – does not require the use of exogenous BV (unlike IFP1.4) and, as a result, demonstrates high brightness in animal cells. Owing to this, iRFP713 has found wide application for *in vivo* visualization of various cells and tissues and is now accepted as a reference standard for the newly developed NIR FPs (see table). The rest of proteins in this series (iRFP670, iRFP682, iRFP702, iRFP720) [12] also demonstrate high affinity to BV and high fluorescence brightness in cells comparable to those of iRFP713 (table). The use of the iRFP provided the possibility of multicolor labeling and visualization of cells and tissues in the NIR spectral range [12].

The search for other protein molecules suitable for the NIR FP development continues. Recently, a new NIR FP was generated based on the allophycocyanine (APC) from the cyanobacterium *Trichodesmium erythraeum*. Native APC uses PCB as a chromophore. By performing several rounds of random mutagenesis and targeted selection, a protein named smURFP was generated that is capable of binding BV instead of PCB [20]. smURFP is spectrally identical to iRFP670 but exhibits approximately 2-times higher molecular brightness. However, because of the low BV binding constant shown by the apo-form of this protein, it performs significantly poorer comparing to other NIR FPs with regard to brightness when expressed in HeLa cells (only 2% of the iRFP713 brightness under the same conditions) [21].

Monomeric NIR FPs. Despite a wide use of proteins from the iRFP and IFP families for cell and tissue labeling in the studies of malignant tumor development, tissue regeneration, and spread of parasitic infections in an organism, the tendency of these proteins for dimerization limits their applications that require the labeling of individual target proteins for investigating various intracellular processes. It is known that biomarker dimerization could interfere with the normal function of the labeled protein and cause protein aggregation [24], reorganization of organelles [31], and other artifacts [32]. The monomeric structure of a biomarker is especially important for the development of reporters based on Förster resonance energy transfer (FRET) [33], as well as other biosensors. Significant efforts in the creation of NIR FPs went into development of spectrally different, bright, and at the same time, monomeric proteins.

In *in vitro* experiments, IFP1.4 [13] and its improved version IFP2.0 [17] were characterized as monomers; however, their tendency to form dimers was demonstrated later [24, 34]. Proteins from the Wi-Phy series [18, 19] generated at the same time were also characterized as monomers *in vitro*, although their behavior during expression in cells was not investigated.

The first monomeric NIR FPs – mIFP [24] and iBlueberry [25] – were produced using the bacteriophytochrome from *Bradyrhizobium*. The CBD of this protein does not participate in dimer formation which is a characteristic of the full-size protein. The NIR FPs in this series display low affinity to BV and, as a result, were ranked below the dimeric iRFP in brightness in cells (table). The use of mIFP and iBlueberry *in vivo* requires introduction of the exogenous cofactor [21].

Three monomeric proteins, miRFP670, miRFP703, and miRFP709, were generated by engineering of the *Rp*BphP1 phytochrome from *R. palustris* using the available data on its structure [29]. Monomerization of the *Rp*BphP1 phytochrome CBD was achieved by mutagenesis of the C-terminal α-helical fragment of the GAF domain, which together with the α-helical fragments of the PHY and effector domains form the site for the monomer interactions in the protein dimer. Based on successful evolution of *Rp*BphP1, substitutions ensuring protein monomerization were introduced to the C-terminal α-helix in the GAF domain of the dimeric iRFPs, which allowed to produce a whole series of monomeric proteins spectrally identical to their dimeric variants (Fig. 2) [28, 30]. The miRFP proteins retained high brightness characteristic for the dimeric iRFPs (table) due to the high specificity and affinity to BV, which made them promising agents for application in the super-resolution multicolor microscopy and visualization of molecular processes in cells.

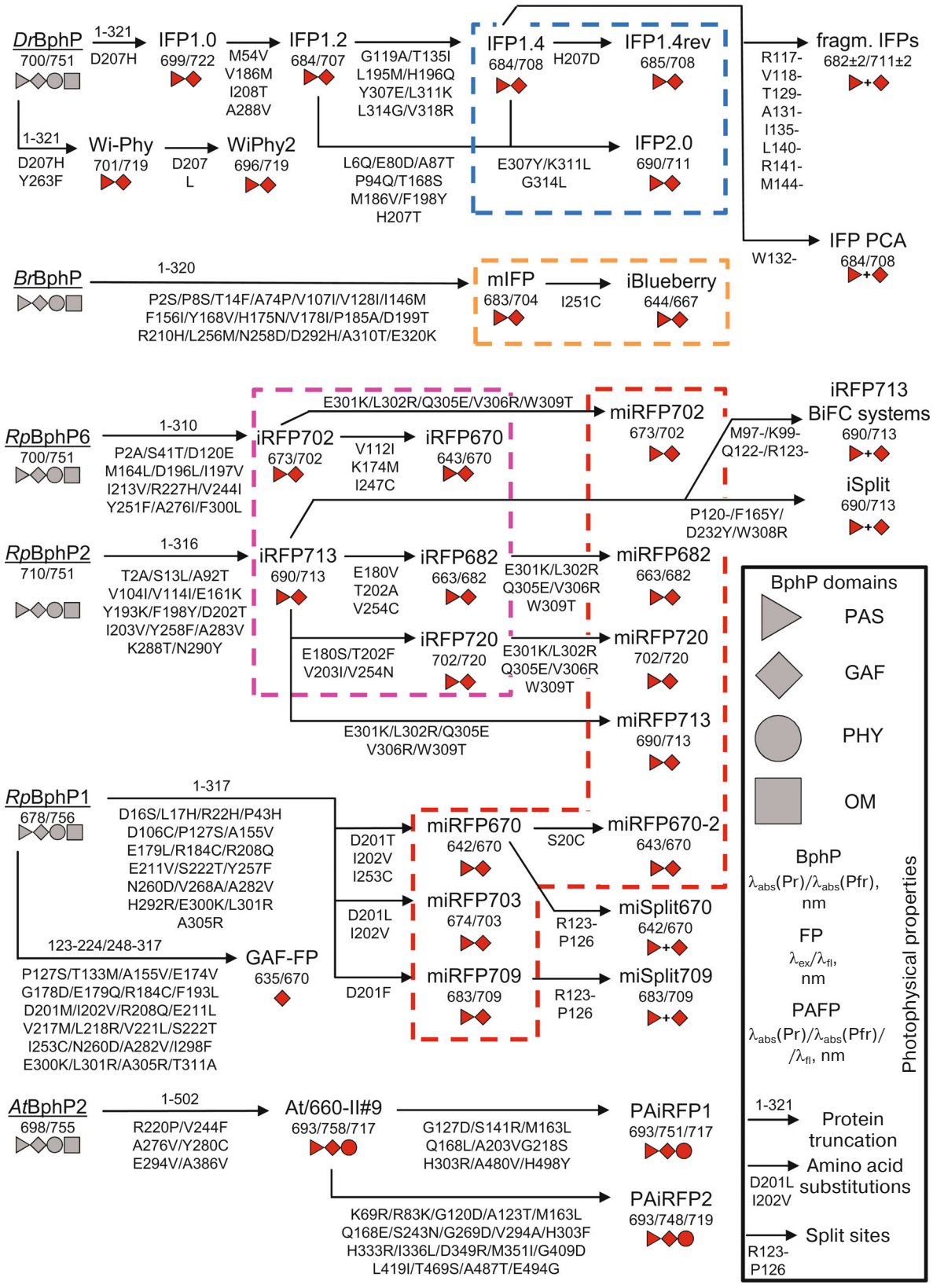

Fig. 2. Molecular evolution of NIR FP derived from BphP. Numbering of amino acid substitutions is given according to the sequence of the template protein (underlined) in each molecular phylogenetic tree. Domain structures of FP and native BphP are shown in red and grey, respectively. IFP family is marked with blue dashed line, mIFP family – orange dashed line, iRFP family – purple dashed line, and miRFP family – red dashed line.

The family of NIR biomarkers produced from *Rp*BphP1 also includes the monomeric single-domain GAF-FP [26], which has the lowest molecular mass (19.6 kDa) among the BphP-based NIR biomarkers. Spectral characteristics of GAF-FP are identical to those of miRFP670. Molecular evolution of GAF-FP negatively affected the affinity and specificity of BV binding by the protein. GAF-FP binds PCB more efficiently than BV and demonstrates low brightness during expression in HeLa cells in the absence of exogenous BV.

Several monomeric NIR FPs termed BDFPs were derived from the phycobilisome core subunit ApcF2 from the thermophilic cyanobacterium *Chroococcidiopsis thermalis* [22]. Using molecular evolution, the natural specificity of ApcF2 to PCB was changed in such a way that BDFPs acquired the ability to bind BV. The disruption of the region involved in the dimerization of the original ApcF2 protein resulted in a slightly reduced brightness of monomeric BDFPs (see table). BDFPs display spectral characteristics that are similar to those of iRFP713. They have small size (~15 kDa), excellent photo- and thermal stability, and high resistance to the denaturing conditions mediated by chemical agents and low pH values (down to pH 2). The authors suggested that the high stability of BDFPs would allow their use for visualization of molecular processes under acidic conditions typical for certain organelles (lysosomes) and tissues (gastrointestinal tract). BDFPs demonstrate detectable fluorescence during expression in *Lactobacillus lactis* cells cultivated in the medium with pH 3. However, the brightness of BDFPs expressed in mammalian cells does not exceed the brightness of smURFP (table). BDFPs have not been yet characterized *in vivo*.

MOLECULAR ENGINEERING OF NIR FPs

Phytochromes are photoreceptors involved in the regulation of cell signaling pathways induced by light. Phytochromes detect light via the light-sensitive photosensory core module (PCM) containing covalently bound chromophore and transmit this signal to the output effector module (OM) that initiates cellular response. The chromophore in BphP is the linear tetrapyrrole BV; cyanobacterial and plant phytochromes form complexes with PCB and phytochromobilin, respectively [15]. The domain structure of PCM in BphP is highly conserved and includes PAS (Per–ARNT–Sim), GAF (cGMP phosphodiesterase–adenylate cyclase–FhlA), and PHY (phytochrome-specific) domains connected by α-helical linkers (Fig. 3a) [15, 35, 36]. In BphP, the natural chromophore BV is covalently bound to the conserved cysteine residue in the *N*-terminal region of the PAS domain and embedded into the pocket of the GAF domain (Fig. 3b) [37-39]. Chromophores of cyanobacterial and plant phytochromes form covalent bond with the conserved cysteine residues in the GAF domain [15]. The PHY domain is considered to be involved in transmission to the OM of the structural changes occurring during chromophore photoisomerization under the action of light (Fig. 3a) [36, 40].

Light absorption by BphP causes chromophore photoisomerization, which in turn, induces a number of changes in the protein structure that result in protein activation. In order to produce fluorescent proteins based on BphP, one must first block the process of chromophore photoconversion, as well as other pathways of non-radiant dissipation of chromophore excitation energy. The

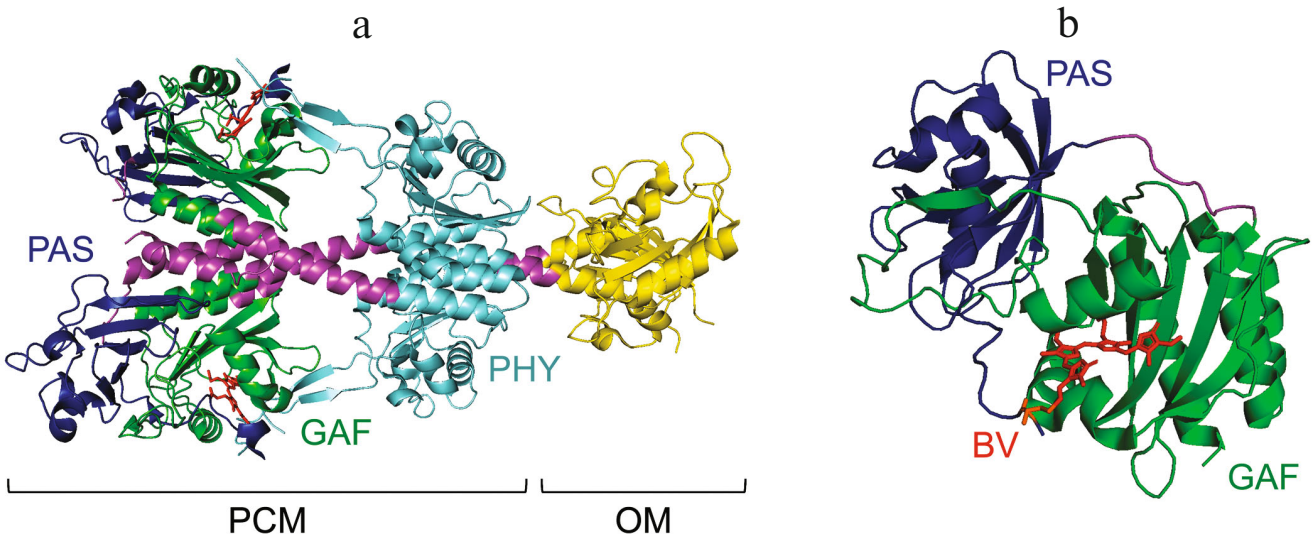

Fig. 3. Three-dimensional structures of (a) BphP (XccBphP, PDB: 5akp [126]) and (b) NIR FP (miRFP703, PDB: 5vik [45]). Blue, PAS domain; green, GAF domain; turquoise, PHY domain; yellow, OM; magenta, linkers connecting domains. BV chromophore (red) is located in the GAF domain pocket and linked by covalent bond to the conserved cysteine residue (orange) in the *N*-terminal extension of the PAS domain.

design of NIR FPs is based on the inhibition of photoconversion via interrupting the key interaction between Asp207 residue (numbering of amino acids is according to the *Dr*BphP sequence) in the conserved PXSDIP motif of the GAF domain and conserved Arg472 in the PHY domain, which can be realized by removal of the PHY domain and the OM from BphP [41]. Mutagenesis of the CBD consisting of two domains (PAS and GAF) demonstrated that substitution of Asp207, Ile208, and Tyr263 in the microenvironment of the chromophore can provide inhibition of the non-radiant dissipation of the chromophore excitation energy [18, 42]. Analysis of the *Dr*BphP-based NIR FPs revealed that the increase in their fluorescence quantum yield is related to the increase in chromophore rigidity. Introduction of hydrophobic Leu instead of the polar Asp207 in the Wi-Phy protein resulted in the decrease of the amount of bound water in the protein chromophore-binding pocket, which affected the network of hydrogen bonds between the pyrrole rings of the chromophore and amino acid residues in its microenvironment, thus inhibiting proton transfer in the chromophore excited state and decreasing the mobility of the chromophore D-ring [19]. Using the molecular dynamics technique and the data on the 3D structures of *Dr*CBD and a number of IFPs, the possibility of water molecule exchange between the GAF domain pocket containing chromophore and the surrounding solvent was demonstrated, which affects the network of hydrogen bonds between the chromophore and amino acids in its microenvironment, as well as chromophore conformation [43]. It was shown that either Thr207 with bulky hydrophobic methyl group or large His207 can efficiently prevent water access to the chromophore-binding pocket of IFPs. Furthermore, the imidazole ring in His207 can experience fast rotations, thus distorting the planar configuration of the chromophore. This explains why IFP2.0 with Thr207 has higher fluorescence quantum yield than IFP1.4 containing His207 (table). These data indicate that insertion of the His residue into position 207 is not essential for the generation of NIR FPs with a high quantum yield. The highest quantum yield among the IFPs was observed for IFP1.4rev (8.7%) that contains the reverse substitution of His207 with Asp [44]. Studies of the spectral properties of the iRFP713 mutant variants containing substitutions reverse to those introduced during the development of this *Rp*BphP2-based biomarker revealed that substitutions of amino acids distant from the chromophore also affect the protein quantum yield [42].

It must be mentioned that when developing photoactivated NIR biomarkers, the PHY domain must be preserved to maintain protein ability for the light-induced conversion from the inactive non-fluorescent state to the fluorescent one. In particular, dimeric PAiRFPs were produced on the basis of the *At*BphP2 phytochrome from *Agrobacterium tumefaciens* C58 (table and Fig. 2) [23] that could be activated by the light with a wavelength of 660 nm.

It became clear during the development of NIR FPs that proteins produced in bacteria in the presence of BV excess do not always retain their brightness when expressed in mammalian cells (table). One of the reasons could be a reduced specificity for BV binding. It was shown in the investigations of the fluorescence properties of the *Dr*BphP mutant forms [41] that proteins of the IFP and Wi-Phy series containing His207 residue instead of Asp207 bound not only BV, but also protoporphyrin IX present in mammalian cells, while *Dr*BphP-based NIR FPs containing Leu207 interacted with BV with a high specificity [19].

It was demonstrated using miRFP670 as an example that the specificity to BV could be increased by substitution with Ala of several Ser residues close to the Cys residue participating in the chromophore covalent binding [45]. The produced mutant protein miRFP670/AAANCEA was found to be the brightest among the generated miRFPs (its brightness during expression in mammalian cells was 238% of the iRFP713 brightness).

Studies of the spectral properties of NIR FPs provided the basis for understanding the mechanisms responsible for their spectral variety. In the first NIR FPs engineered from *Dr*BphP [13] and *Rp*BphP2 [11], BV was covalently bound to the Cys15 residue (Cys^{PAS}; Fig. 4a) at the *N*-terminus of the PAS domain (amino acid numbering is accordingly to the *Rp*BphP2 sequence). An alternative covalent binding of BV to the Cys residue inserted into the conserved SPXH motif in the GAF domain (Cys^{GAF}; Fig. 4b) is possible, which results in the hypsochromic shift in the absorption and fluorescence spectra of the resulting NIR FPs by 30-40 nm relative to the spectral characteristics of NIR FPs with the conserved Cys in the PAS domain [25, 27, 46]. The data of X-ray diffraction analysis and mass spectrometry obtained for the BphP1-FP with Cys residue only in the GAF domain demonstrated that the hypsochromic shift of the absorption and fluorescence spectra of the chromophore covalently bound to the Cys^{GAF} was due to the shorter π-conjugated system in comparison with the BV-Cys^{PAS} chromophore. It was shown that in BphP1-FP, BV could be linked to Cys^{GAF} via $C3^1$ or $C3^2$ carbon atoms of the pyrrole ring A side chain, both chromophore derivatives being spectrally identical [27]. Two suggestions have been made to explain the high quantum yield of NIR FPs with the fluorescence spectra displaying hypsochromic shift: (i) the chromophore bound to Cys^{GAF} has more rigid structure due to the limited mobility of the pyrrole ring A; (ii) mobility of the ring A does not affect the properties of BV-Cys^{GAF}, because in this case, it is not included in the conjugated system of π-bonds [47]. Chromophore interaction with dimeric NIR FPs is complicated by intermonomer allosteric effect, with a number of spectral characteristics being sensitive to this effect. It was shown that in the dimeric NIR FPs containing Cys residues in the GAF domains but not in the PAS domains, covalent

binding of BV to one of the monomers inhibits covalent binding of BV to the other monomer [46], which results in the emergence of the long-wavelength shoulder in the absorption and fluorescence spectra of such dimeric NIR FPs. In the dimeric NIR FPs containing Cys residues in both PAS and GAF domains, BV is covalently bound to Cys^{GAF} in both monomers; as a result, these variants demonstrate high fluorescence quantum yield and narrow absorption and fluorescence spectra. It was shown using the proteins of the miRFP series that BV could form covalent bonds simultaneously with Cys^{PAS} and Cys^{GAF} (Fig. 4c) [45]. It was suggested that such cross-linking of the PAS and GAF domains via BV could be the reason for high structural stability of NIR FPs containing Cys residues in both PAS and GAF domains [48, 49].

Several more amino acid substitutions have been identified that change the spectral properties of NIR FPs. The Val186Met substitution in NIR FPs based on *Dr*BphP results in a 10-nm hypsochromic shift in the absorption and fluorescence spectra [44]. The absorption and fluorescence spectra of miRFP709 and miRFP703 differing by two amino acid substitutions (see Fig. 2) and containing Phe and Leu, respectively, in position 201 (numbering of amino acids for *Rp*BphP1) are shifted relatively to each other by 9 and 6 nm, respectively. The X-ray diffraction data obtained for miRFP709 allowed the suggestion that introduction of aromatic amino acids into the chromophore microenvironment in such a way that their side radicals could participate in the π-stacking interactions with BV could cause bathochromic shift in the absorption and fluorescence spectra [45].

It is often essential to use truly monomeric biomarkers for labeling cellular proteins, especially in the studies of protein–protein interactions (PPIs). The obvious strategy for creating monomeric NIR FPs is a search and engineering of BphP that are monomeric in their native form or can be easily transformed into this state by the removal of the PHY domain and the OM. For example, in order to create mIFPs, authors conducted the database search with subsequent analysis of protein regions corresponding to the dimerization interface of the *Dr*BphP. As a result, the *Br*BphP protein was identified that contains polar Thr instead of the hydrophobic Leu in this position, which eliminates the possibility of strong hydrophobic interactions between the monomers at this site [24]. The generation of three monomeric NIR FPs from *Rp*BphP1 [29] became possible due to the fact that the dimerization interface in the full-size protein is formed predominately by the PHY domain and the OM [50]. Considering that generation of FPs from BphP implies removal of these domains, the remaining PAS-GAF fragments behave as monomers [29]. Another strategy involves mutagenesis of dimeric NIR FPs in aim to disrupt the sites of monomer interaction in the dimer while preserving their photophysical characteristics. Rational evolution of the dimeric interface in iRFP720 resulted in the generation of the monomeric NIR FP with the largest bathochromic shift of the fluorescence spectrum observed to date [30]. The reduction of the molecular mass of NIR FP from 35 kDa, which is typical for CBD, to 19.6 kDa was achieved by the development of GAF-FP consisting of the GAF domain only [26]. The authors transferred the Cys residue required for the BV binding from the *N*-terminus of the PAS domain to the position corresponding to the Cys residue that covalently binds chromophores in the GAF domain of cyanobacterial and plant phytochromes. However, subsequent removal of the PAS domain resulted in destabilization of the protein structure accompanied by formation of visible aggregates. It was possible to stabilize the structure by removal of the loop participating in the formation of the knot structure in the polypeptide chains of PAS and GAF domains in BphP, but which is absent in stable cyanobacteriochromes [26].

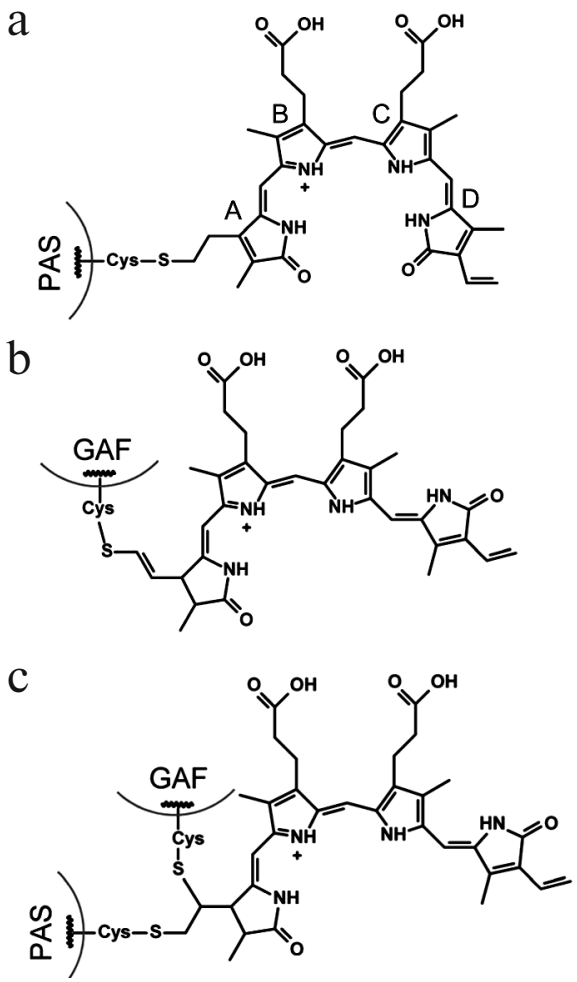

Fig. 4. Chemical structures of different derivatives of the BV chromophore (pyrrole rings A-D are shown) in NIR FPs (a-c). Adapted from [45] with permission from The Royal Society of Chemistry, Creative Commons Attribution-NonCommercial 3.0 license.

The two-domain structure of the BphP-based NIR FPs significantly simplifies the task of PPI reporter development. However, it must be taken into account that BphP contains an unusual structural element, figure-of-eight knot, formed by the *N*-terminal part of the PAS domain and disordered loop of the GAF domain [35]. It was shown for iRFP713 and IFP1.4 that the cleavage sites can be introduced mainly in the *N*-terminal disordered region of the PAS domain, disordered loop between the PAS and GAF domains, GAF domain α-helix adjacent to this loop, and in the loops between the β-strands in the PAS domain [51, 52]. NIR FPs do not tolerate circular permutations between the sites in the GAF domain loop participating in the knot formation [52]. These data argue for that some PPI reporters based on iRFPs and IFPs may fold into the knotted structure (typical for the native protein) at reconstruction from the two protein fragments. However, some data contradict this suggestion. For example, the PPI reporter iSplit (Fig. 2) derived from iRFP713 displays lower intracellular stability in comparison with the original NIR FP [53]. The knots were proposed to retard the translocation through the proteasome pore of the knot-containing proteins, thus increasing its stability in the cell [54, 55]. In addition, it was shown that IFP PCA, a PPI reporter consisting of two fragments of IFP1.4 (Fig. 2), was capable of reversible association [56]. The proteins containing knots would hardly dissociate, because it was shown that knots are preserved in chemically denatured proteins [57]. The reversibility of association of the IFP PCA components probably arises from the noncovalent binding of BV.

APPLICATION OF NIR FLUORESCENT BIOMARKERS, REPORTERS, AND BIOSENSORS

NIR FPs have been used in a wide variety of fundamental and applied studies in biology and medicine. Due to the NIR fluorescence, the main area of NIR FP application is labeling of cells and tissues for visualization of biological processes *in vivo*. One of the most popular biomarkers is iRFP713 due to its high brightness in cells, low cytotoxicity, and stable expression in mammalian cells [5, 6, 11, 12, 25, 29, 58-83]. Based on iRFP713, several high-throughput systems for counting and analyzing cells in culture have been developed that can be used for screening of compounds with antitumor activity and therapeutic preparations [63, 74]. Low cytotoxicity of iRFP713 allowed generation of transgenic rat and mouse strains with high expression of this biomarker in all tissues, including nervous, cardiovascular, and digestive systems [5, 64, 69, 75]. Besides mammals, the list of organisms demonstrating successful expression of NIR FP includes bacteria (*Escherichia coli*, *Lactococcus lactis*, several strains of *Lactobacillus*) [11-13, 22, 24, 26, 29, 59], yeast (*Saccharomyces cerevisiae*, *Kluyveromyces lactis*, *Pichia pastoris*) [56], Protozoa (several strains of *Leishmania*) [60, 73], insects (*Drosophila melanogaster*) [17, 24, 64, 84], nematodes (*Caenorhabditis elegans*) [22], and fish (*Danio rerio*) [24, 25].

Because of their spectral properties, NIR FPs can be used in combination with fluorescent markers and optogenetic tools operating in the visible spectral range [65, 66, 76, 85, 86]. For example, iRFP670 was used in combination with mCherry and the OptoSTIM1 optogenetic tool allowing regulation of the intracellular calcium levels with the help of blue-light irradiation [86]. The chimeric protein consisting of iRFP713 and a fragment of the PLCδ_1 pleckstrin homology domain was used for investigating the dynamics of phosphatidylinositol 4,5-bisphosphate on the cell membrane during its dephosphorylation by optogenetic cryptochrome CRY2-based tools controlled with the blue light [65]. The movement of nuclei was monitored using iRFP713 upon optogenetic stimulation of the muscle cell contraction with ChR2 [76].

It must be noted that because the vast majority of biosensors and optogenetic tools used in neurobiology operate in the visible spectral range, the use of NIR FPs seems especially promising. Although, due to the low level of BV in neurons, their visualization using biomarkers with a moderate affinity to BV, such as NIR FPs from the IFP, mIFP, and smURFP series, requires introduction of exogenous BV or co-expression of HO [17, 20, 24, 29]. However, the use of NIR FPs from the iRFP and miRFP series with a relatively high affinity to BV eliminated the need for exogenous BV in the labeling of primary hippocampal neurons [29, 87], retinal neurons [88], and mouse and rat cortical neurons *in vivo* [75, 81, 87]. One must take into account that in an organism, BV participates in the cell defense against oxidative stress [89] and activation of signaling pathways [90-92], as well as affects cell viability and proliferation [93]. HO plays a key role in heme catabolism, and its overexpression can affect cell physiology [94-96]. Hence, an increase in the BV concentration above the physiological levels or co-expression of HO can lead to artifacts and unwanted metabolic consequences in the cell culture or *in vivo*.

The main advantages of NIR FPs in visualization of various processes in animal tissues and organs are efficient transmission of the excitation/fluorescence light through biological tissues and low autofluorescence of the tissues in the NIR range of the spectrum. Stability and low cytotoxicity of NIR FPs allow using these biomarkers for prolonged visualization of cells in organism and monitoring of their migration in the body in pathological processes in animal models. Expression of iRFP713 in cardiomyocyte precursors provided the opportunity to observe the process of heart muscle regeneration in ischemia in mice [6]. Hematopoietic stem cells labeled with iRFP713 were successfully used for monitoring the restoration of blood cell population in irradiated mice [5]. iRFP713 have been extensively used for investigating the

growth and metastasis of various tumors, e.g., inflammatory breast cancer [58], breast adenocarcinoma [83], primary melanoma [67], and prostate cancer [82] in animal models. iRFP720 was used to study metastasis of prostate cancer in bones of live mice [97]. Proteins from the iRFP series have been successfully used for visualization of tumors of internal organs of live mice [11, 12, 68, 79, 98]. The use of photoactivated PAiRFP proteins allowed to significantly increase the image contrast owing to the signal registration from the two states of PAiRFP during visualization of tumors at the early stages of their development in mice [23].

iRFP670 was used for evaluating the efficiency of the new method for delivery of small interfering RNAs (siRNAs) into intracranial glioblastoma cells in mice [99]. For this purpose, glioblastoma cells were generated that stably expressed a chimeric protein consisting of iRFP670 and protein target of the siRNA. Hence, the efficiency of the siRNA delivery and siRNA interference with mRNA was estimated quantitatively and in real time from the decrease in the fluorescent reporter signal.

Strains of transgenic mice [64] and rats [75] were generated that expressed iRFP713 under control of the Cre recombinase. It was shown that the presence of one iRFP713 allele (a condition required for the generation of mouse derivative strains via hybridization) was sufficient for efficient visualization [64]. Transgenic mice with inducible expression of iRFP713 were used for studying the development of lung and pancreatic cancers (Fig. 5) [64].

Bioluminescence methods are often more sensitive in comparison to the ones based on fluorescence due to the low background signal. Chimeric NIR luciferases iRFP670–RLuc8 and iRFP720–RLuc8 that combine the advantages of bioluminescence and NIR fluorescence were used for multicolor visualization of the growth and metastasis of breast adenocarcinoma *in vivo* (Fig. 6) [100]. Migration of human mesenchymal stem cells after their transplantation to the mouse cerebral cortex was visualized using chimeric luciferase luc2–iRFP720 [101]. Stability and low toxicity of this biomarker in combination with high sensitivity of the method allowed detection of low numbers of these cells ($1 \cdot 10^5$) within a period of 7 weeks.

Labeling of viral particles and parasitic microorganisms with NIR FPs offers the opportunity to investigate the spread of infection in a model organism and potentially can be used for testing new therapeutic agents. *Leishmania* cells expressing iRFP713 [60, 73], influenza A virus with introduced iRFP713 gene [77], and rabies virus with introduced iRFP670 and iRFP720 genes [102] were used for studying the pathologies with different etiology in live mice.

Spectrally different NIR FPs can be used for simultaneous visualization of several tissues and organs. It was demonstrated that up to five cell populations labeled with different iRFPs can be distinguished by flow cytometry using the spectral deconvolution method [103]. Simultaneous *in vivo* visualization of up to five subcutaneous tumors labeled with different iRFPs was carried out using special signal processing algorithms [12]. The use of NIR FP pairs with fluorescence maxima differing by 35 nm and more (such as iRFP670 and iRFP713 or miRFP670 and miRFP709) allows to obtain multicolor

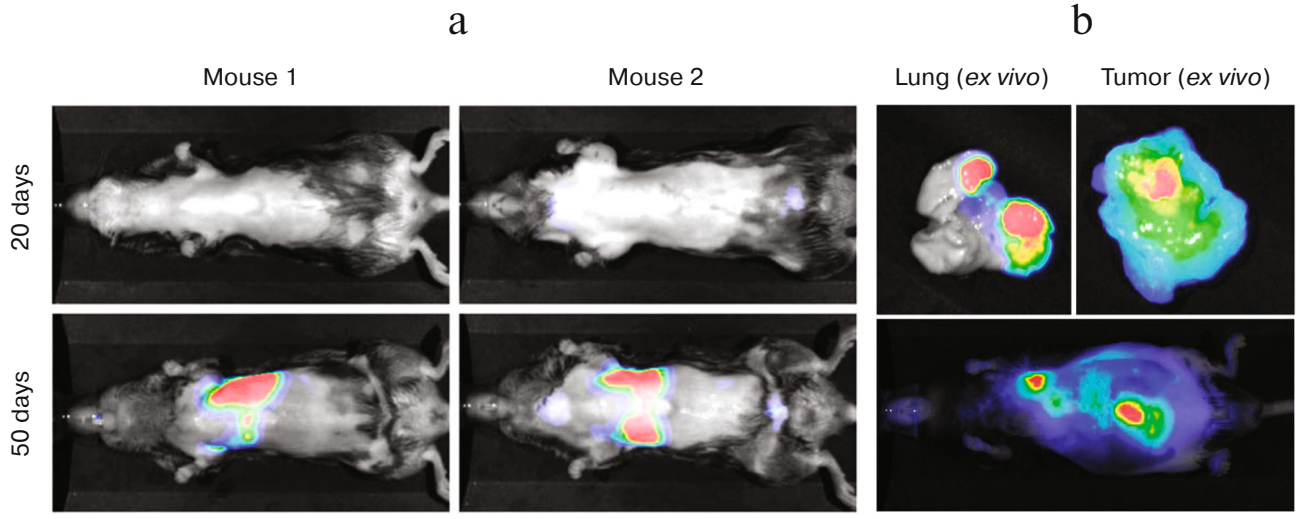

Fig. 5. Visualization of tumor development in transgenic animals using NIR fluorescence: a) lung cancer mouse model; iRFP713 fluorescence recorded 20 (upper panel) and 50 days (lower panel) after intranasal administration of adenoviruses carrying the Cre recombinase gene; b) pancreatic cancer mouse model; metastasis are clearly visible in lungs by the fluorescence of iRFP713 reporter (lower panel); lung and tumor following resection to confirm the signal source (upper panel). Adapted from [64] with permission from Nature Publishing Group, Creative Commons Attribution 4.0 international license.

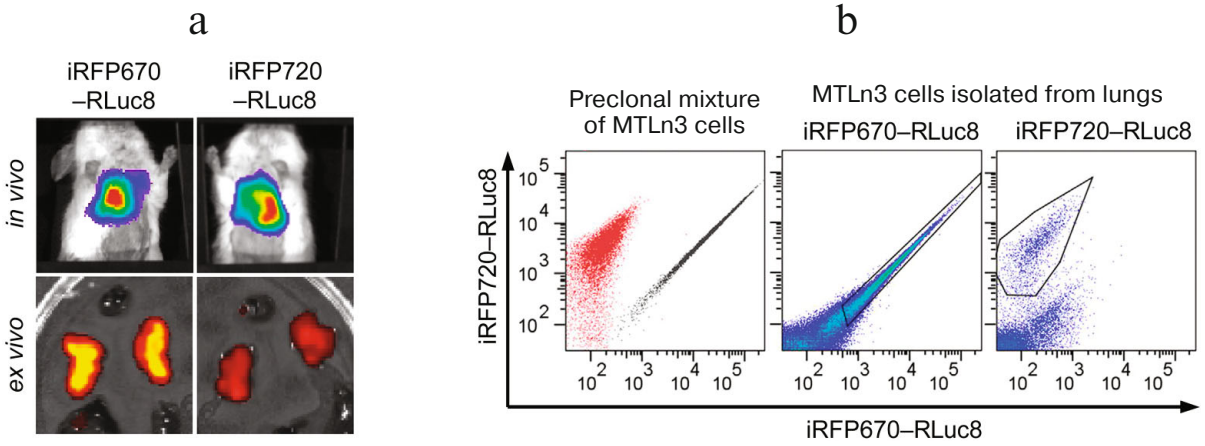

Fig. 6. Metastasis of MTLn3 adenocarcinoma cells expressing chimeric NIR luciferases iRFP670–RLuc and iRFP720–RLuc in mice: a) *in vivo* bioluminescence imaging (upper panel); b) flow cytometry of the mixture of MTLn3 cells used for injection into mouse mammary glands (on the left, the signals from iRFP670–RLuc8 and iRFP720–RLuc8 are shown in red and grey, respectively) and cells isolated from lung tissue 4 weeks after injection. Adapted from [100] with permission from Nature Publishing Group, Creative Commons Attribution 4.0 international license.

images of cells and organs in the NIR region without using complicated signal processing procedures [12, 25, 29, 59].

By supplementing monomeric GFP-like proteins, monomeric NIR FPs significantly expanded the color palette of markers suitable for labeling individual proteins. Monomeric mIFP and proteins of the miRFP series were used together with TagGFP2 and mCherry to produce high-resolution images by the multicolor structured illumination microscopy (SIM) [24, 29]. Monomeric BDFP [22] also demonstrated high photostability when used in SIM.

NIR FP-based reporters and biosensors. Numerous biosensors and reporters of various molecular biological processes have been developed based on the GFP-like proteins. However, application of these constructs *in vivo* has been challenging due to the fact that they fluoresce in the visible range of the spectrum. NIR biosensors offer the same advantages as NIR biomarkers because of low scattering and absorption of NIR light in animal tissues. Expansion of the color palette of available biosensors provides additional opportunities for multicolor labeling.

Identification of PPIs contributes to the understanding of the function of interacting proteins, their localization, participation in signaling, and formation of protein complexes. PPI reporters consist of two fragments of the sensor protein, which are fused with the target proteins and generate or change the output signal upon the target proteins interaction or their co-localization in the cell. The main approaches for investigating PPIs are based on bimolecular fluorescence complementation (BiFC) and FRET. BiFC reporters consist of two non-fluorescent fragments of a fluorescent marker that are fused to the target proteins. When the target proteins are in a close proximity, this reconstitutes the native structure of the fluorescent biomarker and results in fluorescence emergence [104-106]. FRET biosensors use FRET pairs of intact biomarkers [107-109].

The two-domain structure of NIR FPs was found to be suitable for the development of BiFC-based PPI reporters. The first NIR PPI reporter named iSplit was produced by separating iRFP713 into individual PAS and GAF domains using directed mutagenesis (Fig. 2) [53]. iSplit displays high contrast in BiFC; the re-assembled structure of iSplit to a large degree retains the photophysical properties of the native protein, including its high affinity to BV. Later, several variants of iRFP713 BiFC reporters were created [110] (Fig. 2) with another positions of the split site that exhibited lower contrast *in vivo* in comparison with iSplit [110]. Re-assembly of iSplit and iRFP713 BiFC reporter is irreversible, which is typical for the majority of PPI reporters based on the GFP-like proteins [104].

Using the known structure of *Dr*BphP, new IFP1.4-based PPI reporters have been generated: IFP PCA (protein complementation assay) [56] and a set of fragmented IFPs [51] (Fig. 2). Experiments in mammalian cells demonstrated that fluorescence complementation of IFP PCA was reversible. Fragmented IFPs have not been tested in mammalian cells. These reporters inherited the drawbacks of IFP1.4 – namely, the requirement of exogenous chromophore and low brightness upon expression in animal cells.

Spectrally different monomeric PPI reporters named miSplit670 and miSplit709 were produced based on the monomeric proteins miRFP670 and miRFP709, respectively, by breaking the polypeptide chain between the PAS and GAF domains (Fig. 2) [29]. Both systems allow PPI

detection with a high contrast of fluorescence complementation; the re-assembly of the system components is irreversible. Reconstructed miSplit670 and miSplit709 retain more than 40% brightness of the original proteins. The advantage of these systems in comparison with iSplit is a lower background signal due to low self-association. miSplit670 and miSplit709 have the same PAS domain, but different GAF domains containing introduced mutations that determine the spectral properties of the re-assembled proteins. Simultaneous application of miSplit670 and miSplit709 makes it possible to monitor interactions of a protein labeled with the PAS domain with two other proteins labeled with different GAF domains. Due to a high contrast and low autofluorescence, miSplit670 and miSplit709 could be used for RNA detection with a high sensitivity [29].

The first PPI sensor named *Dr*Split was designed on the basis of the *Dr*BphP photosensory module. Assembly of its PAS and GAF-PHY domains results in the formation of a sensor molecule capable of photoconversion between the two states upon illumination with a light of a certain wavelength [111]. Considering that the output signal in this case is ultrasonic waves, the phenomenon has been called bimolecular photoacoustic complementation (BiPC). *Dr*Split was tested in cells and *in vivo* as a fusion with a pair of proteins FRB and FKBP that form heterodimers in the presence of rapamycin. Application of this BiPC reporter allowed to monitor PPIs at a depth of 9.3 mm in metastasizing tumors (Fig. 7) and mouse liver with a spatial resolution of 125 μm and sensitivity limit of 530 cells [111].

Several reporters have been designed for monitoring protease activity in the cells during apoptosis. The NIR biosensor iProtease was generated by rational design and circular permutation of the mIFP sequence. The cleavage site was introduced into the produced mIFP-based structure in such a way that the non-cleaved reporter do not bind the chromophore [84]. The iCasper reporter activated by caspases 3 and 7 was also generated in this study and used for apoptosis visualization in *Drosophila* larvae dur-

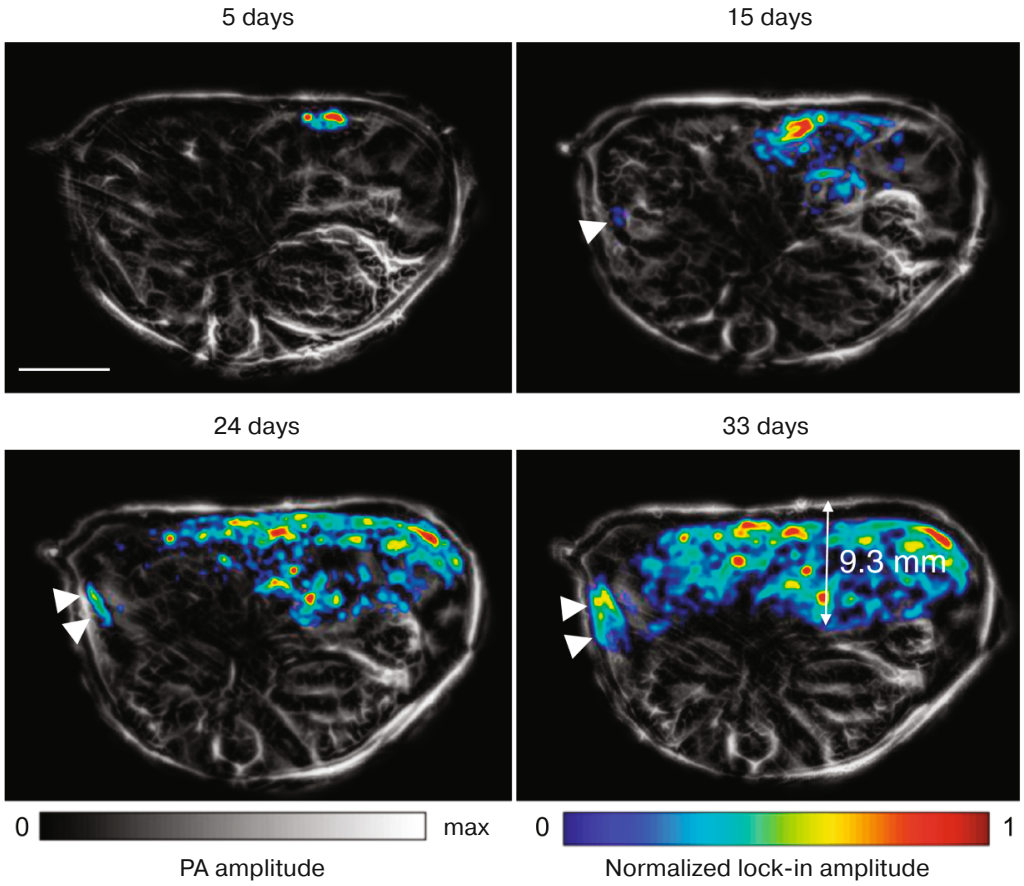

Fig. 7. Visualization of protein–protein interactions in a growing and metastasizing tumor in a mouse liver by RSPACT. Adenocarcinoma cells expressing *Dr*Split (rapamycin sensor) were injected into mouse liver. Rapamycin was injected into the mouse tail vein ~40-44 h prior to acquiring each image. White arrows show the secondary tumors. Anatomic image is presented in black and white; the photoacoustic signal from the sensor is shown using a pseudocolor scale. Scale bar, 5 mm. Adapted from [111] with permission from the Nature Publishing Group, Creative Commons Attribution 4.0 international license.

ing morphogenesis and oncogenesis. FRET-based apoptosis sensors were constructed that consisted of the far-red GFP-like proteins (mKate2 or eqFP650) linked to the NIR FP iRFP713 via the protease-sensitive linker [112].

Monomeric miRFP670 and miRFP720 form an efficient FRET pair [30] that can be used for designing FRET biosensors absorbing and fluorescing in the NIR range. Thus, these proteins were used for the development of a NIR biosensor of the Rac1 GTPase activity that can be used together with the CFP-YFP FRET biosensors and optogenetic tools activated in the blue-green range of the spectrum [30]. Moreover, the authors generated NIR biosensors to monitor PKA and JNK kinase activities by replacing the CFP-YFP donor-acceptor pair with miRFP670/miRFP720 in the improved versions of the AKAR and JNKAR sensors [109].

NIR reporters for cell cycle monitoring were created using the miRFP670/miRFP709 [29] and IFP2.0/smURFP [20] pairs based on the design and operating principle of the fluorescent ubiquitination-based cell cycle indicator (FUCCI) based on the GFP-like proteins [113]. Cyclic degradation of the Gem and Cdt1 proteins labeled with fluorescent biomarkers and the corresponding changes in fluorescence allow visualization of cell cycle dynamics in real time. NIR cell cycle reporters have been tested in mammalian cells [20, 29] and *in vivo* [29].

A chimeric protein consisting of the non-modified miRFP703 and IκBα, an inhibitor of the NF-κB transcription factor, can be used as a sensor of the NF-κB signaling pathway activation in response to various stimuli such as the presence of bacterial and viral products, tumor necrosis factor α, and other cytokines. Activation of the NF-κB occurs due to IκBα phosphorylation and fast degradation and, hence, can be monitored by the decrease in the fluorescence of miRFP703 [29]. It was demonstrated that acute inflammation in the mouse liver caused a 3-fold decrease in the fluorescence of this sensor *in vivo*.

NIR FLUORESCENT PROTEINS IN ADVANCED VISUALIZATION TECHNOLOGIES

The emergence of new visualization technologies and methods is usually related to the development of new molecular tools [114]. Generation of NIR FPs facilitated the development and expansion of technologies for *in vivo* visualization of processes occurring deep in biological tissues.

Fluorescence molecular tomography (FMT) methods allow to obtain a three-dimensional image of an organism [115]. The spatial image in FMT is reconstructed using sequential scanning of the sample. FMT was used to acquire a two-color 3D image of closely located tumor and liver labeled with different iRFPs [12] and to evaluate the effect of therapeutics on the tumor cells expressing iRFP720 [116]. FMT in combination with spectral deconvolution algorithm allowed simultaneous monitoring the passage of two populations of lactic acid bacteria expressing iRFP713 or iRFP682, respectively, through the mouse gastrointestinal tract [59].

Generation of hybrid images using FMT together with the X-ray computed tomography (XCT) and positron emission tomography (PET) allows more accurate localization of the target cells inside the organism. The FMT-XCT and FMT-PET-XCT hybrid technologies were used for visualization of iRFP713-labeled brain glioma cells [61], lung carcinoma [70], and prostate tumor [71] in live mice.

The sensitivity of fluorescence signal detection under conditions of high autofluorescence of tissues can be improved significantly by recording the fluorescence decay curves (time domain method, TD method). This approach is based on the difference between the fluorescence lifetimes of the biomarker and fluorescent molecules in biological tissues. The difference in the lifetimes of different iRFPs offers the possibility for multicolor visualization with the TD method. By using this high-sensitive approach, small numbers ($5 \cdot 10^4$) of iRFP720-expressing cancer cells were detected after their introduction into the mouse lungs [117].

The photoacoustic effect (PA) is a generation of ultrasound waves by the tissues following thermoelastic expansion caused by the absorption of ultrashort light pulses. The PA-based visualization techniques achieve high spatial resolution and allow *in vivo* measurements at a larger depth in comparison with the fluorescent techniques, because ultrasonic waves scatter in tissues even less than the NIR light [118]. The images of the breast tumor located at a depth of 4 mm [62] and glioblastoma in the mouse brain with approximately 0.1-mm resolution [61, 80] were generated with the help of PA tomography using the iRFP713-labeled tumor cells. The method of PA flow cytometry was used for monitoring the cells labeled with iRFP713 in the blood vessels of live mice [72]. The method of PA tomography allowed visualization of two tumors expressing iRFP670 and iRFP720 in a mouse at a depth of 8 mm with a submillimeter resolution [69].

Labeling of tumor cells with two probes – iRFP720 and silica-coated gold nanorods (GNRs) – allowed their visualization by the PA-based method of multispectral optoacoustic tomography (MSOT). Visualization of cancer cells immediately after injection into the mouse heart was carried out using the GNR signal; the fluorescence of iRFP720 was recorded at later stages (up to 40 days after injection) [4]. The MSOT method allowed the real-time monitoring of the white adipose tissue transformation into beige adipocytes during adrenergic stimulation, as well as of associated changes of lipid metabolism in mice [119].

iRFP720 was used as a probe that was delivered into the adipose tissue with the help of an adenovirus vector. The intensity of the signal from iRFP720, whose expression was under control of the *Ucp1* promoter and correlated with the expression of the Ucp1 protein specific for beige adipocytes, reflected the changes in the adipocyte type.

The ability to switch between the two photo states upon exposure to light, which is characteristic of the full-size *Rp*BphP1 [111, 120] and AGP1 [121, 122], as well as *Dr*BphP-based biomarkers [111], was used to increase the sensitivity of the PA tomography method. This modification of PA tomography, named reversibly switchable photoacoustic computed tomography (RSPACT), is based on the construction of differential images in order to reduce the tissue background signal. Implementation of RSPACT with *Rp*BphP1 as a biomarker made it possible to monitor tumor growth and metastasis at the depth up to 10 mm with a ~100-μm resolution [120]. The new NIR photochromic probe *Dr*BphP-PCM was developed based on *Dr*BphP for the use in RSPACT [111], which is twice smaller in size, has faster folding, and provides higher contrast of photo-switching in comparison to *Rp*BphP1. Due to the differences in the signal decay kinetics, *Rp*BphP1 and *Dr*BphP-PCM were used simultaneously for visualization of two different tumors in the mouse liver with a high contrast at a depth of 9.1 mm [111]. Using RSPA microscopy, images of several U87 glioblastoma cell layers were produced with the axial resolution of ~0.4 μm and lateral resolution of ~141 nm [120].

CONCLUSION

The rapid expansion of the diversity of genetically encoded NIR biomarkers and development of imaging techniques associated with them makes it possible to monitor physiological and molecular processes in biological tissues at a relatively large depth with high accuracy and high spatial resolution. NIR FPs offer broad opportunities for imaging at different levels: from labeling of intracellular structures to labeling of tissues and organs in the whole organism. NIR FPs have been already used in various areas including basic studies of cellular processes, *in vivo* monitoring of the development of pathologies of various etiology in animal models, and pre-clinical testing of therapeutic agents in cultured cells and animal models.

Despite the development of spectrally different, bright, monomeric NIR biomarkers, the question remains whether further optimization of photophysical properties of these proteins essential for their application as biomarkers is achievable? Is it possible to generate NIR biomarkers of smaller size, with higher quantum yield and greater bathochromic shift of the absorption and fluorescence spectra relative to currently available NIR FPs using molecular evolution?

We expect the emergence of a series of NIR biosensors for key signaling molecules, including Ca^{2+}, cAMP, GTPases, and kinases that will be based on the bright monomeric new-generation NIR biomarkers. Extension with NIR biosensors of the molecular toolbox that includes biosensors based on GFP-like proteins and optogenetic constructs based on various photosensitive molecules operating in the visible spectral range will provide new opportunities for investigating complex and interconnected cellular processes together with controlling cellular functions, which would be possible due to the increase in the number of labeled biological molecules for simultaneous visualization.

Funding

This work was financially supported by the US National Institutes of Health (projects R35 GM122567 and U01 NS103573), the Seventh Framework Program of European Union (project ERC-2013-ADG-340233), and the Molecular and Cell Biology Program of the Presidium of the Russian Academy of Sciences.

REFERENCES

1. Weissleder, R., and Ntziachristos, V. (2003) Shedding light onto live molecular targets, *Nat. Med.*, **9**, 123-128.
2. Weissleder, R. (2001) A clearer vision for *in vivo* imaging, *Nat. Biotechnol.*, **19**, 316-317.
3. Hong, G., Antaris, A. L., and Dai, H. (2017) Near-infrared fluorophores for biomedical imaging, *Nat. Biomed. Eng.*, **1**, 0010.
4. Comenge, J., Sharkey, J., Fragueiro, O., Wilm, B., Brust, M., Murray, P., Levy, R., and Plagge, A. (2018) Multimodal cell tracking from systemic administration to tumour growth by combining gold nanorods and reporter genes, *eLife*, **7**, e33140.
5. Tran, M. T. N., Tanaka, J., Hamada, M., Sugiyama, Y., Sakaguchi, S., Nakamura, M., Takahashi, S., and Miwa, Y. (2014) *In vivo* image analysis using iRFP transgenic mice, *Exp. Anim.*, **63**, 311-319.
6. Wang, Y., Zhou, M., Wang, X., Qin, G., Weintraub, N. L., and Tang, Y. (2014) Assessing *in vitro* stem-cell function and tracking engraftment of stem cells in ischaemic hearts by using novel iRFP gene labelling, *J. Cell. Mol. Med.*, **18**, 1889-1894.
7. Piatkevich, K. D., Malashkevich, V. N., Morozova, K. S., Nemkovich, N. A., Almo, S. C., and Verkhusha, V. V. (2013) Extended stokes shift in fluorescent proteins: chromophore–protein interactions in a near-infrared TagRFP675 variant, *Sci. Rep.*, **3**, 1847.
8. Li, Z., Zhang, Z., Bi, L., Cui, Z., Deng, J., Wang, D., and Zhang, X.-E. (2016) Mutagenesis of mNeptune red-shifts emission spectrum to 681-685 nm, *PLoS One*, **11**, e0148749.
9. Morozova, K. S., Piatkevich, K. D., Gould, T. J., Zhang, J., Bewersdorf, J., and Verkhusha, V. V. (2010) Far-red flu-

orescent protein excitable with red lasers for flow cytometry and superresolution STED nanoscopy, *Biophys. J.*, **99**, L13-L15.
10. Auldridge, M. E., and Forest, K. T. (2011) Bacterial phytochromes: more than meets the light, *Crit. Rev. Biochem. Mol. Biol.*, **46**, 67-88.
11. Filonov, G. S., Piatkevich, K. D., Ting, L.-M., Zhang, J., Kim, K., and Verkhusha, V. V. (2011) Bright and stable near-infrared fluorescent protein for *in vivo* imaging, *Nat. Biotechnol.*, **29**, 757-761.
12. Shcherbakova, D. M., and Verkhusha, V. V. (2013) Near-infrared fluorescent proteins for multicolor *in vivo* imaging, *Nat. Methods*, **10**, 751-754.
13. Shu, X., Royant, A., Lin, M. Z., Aguilera, T. A., Lev-Ram, V., Steinbach, P. A., and Tsien, R. Y. (2009) Mammalian expression of infrared fluorescent proteins engineered from a bacterial phytochrome, *Science*, **324**, 804-807.
14. Fischer, A. J., and Lagarias, J. C. (2004) Harnessing phytochrome's glowing potential, *Proc. Natl. Acad. Sci. USA*, **101**, 17334-17339.
15. Rockwell, N. C., and Lagarias, J. C. (2010) A brief history of phytochromes, *Chemphyschem*, **11**, 1172-1180.
16. Chernov, K. G., Redchuk, T. A., Omelina, E. S., and Verkhusha, V. V. (2017) Near-infrared fluorescent proteins, biosensors, and optogenetic tools engineered from phytochromes, *Chem. Rev.*, **117**, 6423-6446.
17. Yu, D., Gustafson, W. C., Han, C., Lafaye, C., Noirclerc-Savoye, M., Ge, W.-P., Thayer, D. A., Huang, H., Kornberg, T. B., Royant, A., Jan, L. Y., Jan, Y. N., Weiss, W. A., and Shu, X. (2014) An improved monomeric infrared fluorescent protein for neuronal and tumour brain imaging, *Nat. Commun.*, **5**, 3626.
18. Auldridge, M. E., Satyshur, K. A., Anstrom, D. M., and Forest, K. T. (2012) Structure-guided engineering enhances a phytochrome-based infrared fluorescent protein, *J. Biol. Chem.*, **287**, 7000-7009.
19. Lehtivuori, H., Bhattacharya, S., Angenent-Mari, N. M., Satyshur, K. A., and Forest, K. T. (2015) Removal of chromophore-proximal polar atoms decreases water content and increases fluorescence in a near infrared phytofluor, *Front. Mol. Biosci.*, **2**, 65.
20. Rodriguez, E. A., Tran, G. N., Gross, L. A., Crisp, J. L., Shu, X., Lin, J. Y., and Tsien, R. Y. (2016) A far-red fluorescent protein evolved from a cyanobacterial phycobiliprotein, *Nat. Methods*, **13**, 763-769.
21. Shemetov, A. A., Oliinyk, O. S., and Verkhusha, V. V. (2017) How to increase brightness of near-infrared fluorescent proteins in mammalian cells, *Cell Chem. Biol.*, **24**, 758-766.e3.
22. Ding, W.-L., Miao, D., Hou, Y.-N., Jiang, S.-P., Zhao, B.-Q., Zhou, M., Scheer, H., and Zhao, K.-H. (2017) Small monomeric and highly stable near-infrared fluorescent markers derived from the thermophilic phycobiliprotein, ApcF2, *Biochim. Biophys. Acta*, **1864**, 1877-1886.
23. Piatkevich, K. D., Subach, F. V., and Verkhusha, V. V. (2013) Far-red light photoactivatable near-infrared fluorescent proteins engineered from a bacterial phytochrome, *Nat. Commun.*, **4**, 2153.
24. Yu, D., Baird, M. A., Allen, J. R., Howe, E. S., Klassen, M. P., Reade, A., Makhijani, K., Song, Y., Liu, S., Murthy, Z., Zhang, S.-Q., Weiner, O. D., Kornberg, T. B., Jan, Y.-N., Davidson, M. W., and Shu, X. (2015) A naturally monomeric infrared fluorescent protein for protein labeling *in vivo*, *Nat. Methods*, **12**, 763-765.
25. Yu, D., Dong, Z., Gustafson, W. C., Ruiz-Gonzalez, R., Signor, L., Marzocca, F., Borel, F., Klassen, M. P., Makhijani, K., Royant, A., Jan, Y.-N., Weiss, W. A., Guo, S., and Shu, X. (2016) Rational design of a monomeric and photostable far-red fluorescent protein for fluorescence imaging *in vivo*, *Protein Sci.*, **25**, 308-315.
26. Rumyantsev, K. A., Shcherbakova, D. M., Zakharova, N. I., Emelyanov, A. V., Turoverov, K. K., and Verkhusha, V. V. (2015) Minimal domain of bacterial phytochrome required for chromophore binding and fluorescence, *Sci. Rep.*, **5**, 18348.
27. Shcherbakova, D. M., Baloban, M., Pletnev, S., Malashkevich, V. N., Xiao, H., Dauter, Z., and Verkhusha, V. V. (2015) Molecular basis of spectral diversity in near-infrared phytochrome-based fluorescent proteins, *Chem. Biol.*, **22**, 1540-1551.
28. Verkhusha, V. V., Shcherbakova, D. M., and Baloban, M. (2018) *Monomeric Near-infrared Fluorescent Proteins Engineered from Bacterial Phytochromes and Methods for Making Same*, US patent application 20180044383.
29. Shcherbakova, D. M., Baloban, M., Emelyanov, A. V., Brenowitz, M., Guo, P., and Verkhusha, V. V. (2016) Bright monomeric near-infrared fluorescent proteins as tags and biosensors for multiscale imaging, *Nat. Commun.*, **7**, 12405.
30. Shcherbakova, D. M., Cammer, N. C., Huisman, T. M., Verkhusha, V. V., and Hodgson, L. (2018) Direct multiplex imaging and optogenetics of Rho GTPases enabled by near-infrared FRET, *Nat. Chem. Biol.*, **14**, 591-600.
31. Snapp, E. L., Hegde, R. S., Francolini, M., Lombardo, F., Colombo, S., Pedrazzini, E., Borgese, N., and Lippincott-Schwartz, J. (2003) Formation of stacked ER cisternae by low affinity protein interactions, *J. Cell Biol.*, **163**, 257-269.
32. Day, R. N., and Davidson, M. W. (2009) The fluorescent protein palette: tools for cellular imaging, *Chem. Soc. Rev.*, **38**, 2887-2921.
33. Zacharias, D. A., Violin, J. D., Newton, A. C., and Tsien, R. Y. (2002) Partitioning of lipid-modified monomeric GFPs into membrane microdomains of live cells, *Science*, **296**, 913-916.
34. Shcherbakova, D. M., Baloban, M., and Verkhusha, V. V. (2015) Near-infrared fluorescent proteins engineered from bacterial phytochromes, *Curr. Opin. Chem. Biol.*, **27**, 52-63.
35. Wagner, J. R., Zhang, J., Brunzelle, J. S., Vierstra, R. D., and Forest, K. T. (2007) High resolution structure of *Deinococcus* bacteriophytochrome yields new insights into phytochrome architecture and evolution, *J. Biol. Chem.*, **282**, 12298-12309.
36. Yang, X., Kuk, J., and Moffat, K. (2008) Crystal structure of *Pseudomonas aeruginosa* bacteriophytochrome: photoconversion and signal transduction, *Proc. Natl. Acad. Sci. USA*, **105**, 14715-14720.
37. Lamparter, T., Michael, N., Caspani, O., Miyata, T., Shirai, K., and Inomata, K. (2003) Biliverdin binds covalently to agrobacterium phytochrome Agp1 via its ring A vinyl side chain, *J. Biol. Chem.*, **278**, 33786-33792.
38. Lamparter, T., Carrascal, M., Michael, N., Martinez, E., Rottwinkel, G., and Abian, J. (2004) The biliverdin chromophore binds covalently to a conserved cysteine residue in the N-terminus of *Agrobacterium* phytochrome Agp1, *Biochemistry*, **43**, 3659-3669.

39. Wagner, J. R., Brunzelle, J. S., Forest, K. T., and Vierstra, R. D. (2005) A light-sensing knot revealed by the structure of the chromophore-binding domain of phytochrome, *Nature*, **438**, 325-331.
40. Yang, X., Kuk, J., and Moffat, K. (2009) Conformational differences between the Pfr and Pr states in *Pseudomonas aeruginosa* bacteriophytochrome, *Proc. Natl. Acad. Sci. USA*, **106**, 15639-15644.
41. Wagner, J. R., Zhang, J., von Stetten, D., Gunther, M., Murgida, D. H., Mroginski, M. A., Walker, J. M., Forest, K. T., Hildebrandt, P., and Vierstra, R. D. (2008) Mutational analysis of *Deinococcus radiodurans* bacteriophytochrome reveals key amino acids necessary for the photochromicity and proton exchange cycle of phytochromes, *J. Biol. Chem.*, **283**, 12212-12226.
42. Buhrke, D., Escobar, F. V., Sauthof, L., Wilkening, S., Herder, N., Tavraz, N. N., Willoweit, M., Keidel, A., Utesch, T., Mroginski, M.-A., Schmitt, F.-J., Hildebrandt, P., and Friedrich, T. (2016) The role of local and remote amino acid substitutions for optimizing fluorescence in bacteriophytochromes: a case study on iRFP, *Sci. Rep.*, **6**, 28444.
43. Feliks, M., Lafaye, C., Shu, X., Royant, A., and Field, M. (2016) Structural determinants of improved fluorescence in a family of bacteriophytochrome-based infrared fluorescent proteins: insights from continuum electrostatic calculations and molecular dynamics simulations, *Biochemistry*, **55**, 4263-4274.
44. Bhattacharya, S., Auldridge, M. E., Lehtivuori, H., Ihalainen, J. A., and Forest, K. T. (2014) Origins of fluorescence in evolved bacteriophytochromes, *J. Biol. Chem.*, **289**, 32144-32152.
45. Baloban, M., Shcherbakova, D. M., Pletnev, S., Pletnev, V. Z., Lagarias, J. C., and Verkhusha, V. V. (2017) Designing brighter near-infrared fluorescent proteins: insights from structural and biochemical studies, *Chem. Sci.*, **8**, 4546-4557.
46. Stepanenko, O. V., Baloban, M., Bublikov, G. S., Shcherbakova, D. M., Stepanenko, O. V., Turoverov, K. K., Kuznetsova, I. M., and Verkhusha, V. V. (2016) Allosteric effects of chromophore interaction with dimeric near-infrared fluorescent proteins engineered from bacterial phytochromes, *Sci. Rep.*, **6**, 18750.
47. Hontani, Y., Shcherbakova, D. M., Baloban, M., Zhu, J., Verkhusha, V. V., and Kennis, J. T. M. (2016) Bright blue-shifted fluorescent proteins with Cys in the GAF domain engineered from bacterial phytochromes: fluorescence mechanisms and excited-state dynamics, *Sci. Rep.*, **6**, 37362.
48. Stepanenko, O. V., Stepanenko, O. V., Kuznetsova, I. M., Shcherbakova, D. M., Verkhusha, V. V., and Turoverov, K. K. (2017) Interaction of biliverdin chromophore with near-infrared fluorescent protein BphP1-FP engineered from bacterial phytochrome, *Int. J. Mol. Sci.*, **18**, E1009.
49. Stepanenko, O. V., Stepanenko, O. V., Bublikov, G. S., Kuznetsova, I. M., Verkhusha, V. V., and Turoverov, K. K. (2017) Stabilization of structure in near-infrared fluorescent proteins by binding of biliverdin chromophore, *J. Mol. Struct.*, **1140**, 22-31.
50. Bellini, D., and Papiz, M. Z. (2012) Structure of a bacteriophytochrome and light-stimulated protomer swapping with a gene repressor, *Structure*, **20**, 1436-1446.
51. Pandey, N., Nobles, C. L., Zechiedrich, L., Maresso, A. W., and Silberg, J. J. (2015) Combining random gene fission and rational gene fusion to discover near-infrared fluorescent protein fragments that report on protein–protein interactions, *ACS Synth. Biol.*, **4**, 615-624.
52. Pandey, N., Kuypers, B. E., Nassif, B., Thomas, E. E., Alnahhas, R. N., Segatori, L., and Silberg, J. J. (2016) Tolerance of a knotted near-infrared fluorescent protein to random circular permutation, *Biochemistry*, **55**, 3763-3773.
53. Filonov, G. S., and Verkhusha, V. V. (2013) A near-infrared BiFC reporter for *in vivo* imaging of protein–protein interactions, *Chem. Biol.*, **20**, 1078-1086.
54. Huang, L., and Makarov, D. E. (2008) Translocation of a knotted polypeptide through a pore, *J. Chem. Phys.*, **129**, 121107.
55. Virnau, P., Mirny, L. A., and Kardar, M. (2006) Intricate knots in proteins: function and evolution, *PLoS Comput. Biol.*, **2**, e122.
56. Tchekanda, E., Sivanesan, D., and Michnick, S. W. (2014) An infrared reporter to detect spatiotemporal dynamics of protein–protein interactions, *Nat. Methods*, **11**, 641-644.
57. Mallam, A. L., Rogers, J. M., and Jackson, S. E. (2010) Experimental detection of knotted conformations in denatured proteins, *Proc. Natl. Acad. Sci. USA*, **107**, 8189-8194.
58. Agollah, G. D., Wu, G., Sevick-Muraca, E. M., and Kwon, S. (2014) *In vivo* lymphatic imaging of a human inflammatory breast cancer model, *J. Cancer*, **5**, 774-783.
59. Berlec, A., Zavrsnik, J., Butinar, M., Turk, B., and Strukelj, B. (2015) *In vivo* imaging of *Lactococcus lactis*, *Lactobacillus plantarum* and *Escherichia coli* expressing infrared fluorescent protein in mice, *Microb. Cell Fact.*, **14**, 181.
60. Calvo-Alvarez, E., Stamatakis, K., Punzon, C., Alvarez-Velilla, R., Tejeria, A., Escudero-Martinez, J. M., Perez-Pertejo, Y., Fresno, M., Balana-Fouce, R., and Reguera, R. M. (2015) Infrared fluorescent imaging as a potent tool for *in vitro*, *ex vivo* and *in vivo* models of visceral leishmaniasis, *PLoS. Neglected Tropical Diseases*, **9**, e0003666.
61. Deliolanis, N. C., Ale, A., Morscher, S., Burton, N. C., Schaefer, K., Radrich, K., Razansky, D., and Ntziachristos, V. (2014) Deep-tissue reporter-gene imaging with fluorescence and optoacoustic tomography: a performance overview, *Mol. Imaging Biol.*, **16**, 652-660.
62. Filonov, G. S., Krumholz, A., Xia, J., Yao, J., Wang, L. V., and Verkhusha, V. V. (2012) Deep-tissue photoacoustic tomography of genetically encoded iRFP probe, *Angew. Chem.*, **51**, 1448-1451.
63. Hock, A. K., Lee, P., Maddocks, O. D., Mason, S. M., Blyth, K., and Vousden, K. H. (2014) iRFP is a sensitive marker for cell number and tumor growth in high-throughput systems, *Cell Cycle*, **13**, 220-226.
64. Hock, A. K., Cheung, E. C., Humpton, T. J., Monteverde, T., Paulus-Hock, V., Lee, P., McGhee, E., Scopelliti, A., Murphy, D. J., Strathdee, D., Blyth, K., and Vousden, K. H. (2017) Development of an inducible mouse model of iRFP713 to track recombinase activity and tumour development *in vivo*, *Sci. Rep.*, **7**, 1837.
65. Idevall-Hagren, O., Dickson, E. J., Hille, B., Toomre, D. K., and De Camilli, P. (2012) Optogenetic control of phosphoinositide metabolism, *Proc. Natl. Acad. Sci. USA*, **109**, E2316-E2323.
66. Ishii, T., Sato, K., Kakumoto, T., Miura, S., Touhara, K., Takeuchi, S., and Nakata, T. (2015) Light generation of

intracellular Ca^{2+} signals by a genetically encoded protein BACCS, *Nat. Commun.*, **6**, 8021.
67. Jiguet-Jiglaire, C., Cayol, M., Mathieu, S., Jeanneau, C., Bouvier-Labit, C., Ouafik, L., and El-Battari, A. (2014) Noninvasive near-infrared fluorescent protein-based imaging of tumor progression and metastases in deep organs and intraosseous tissues, *J. Biomed. Opt.*, **19**, 16019.
68. Kamensek, U., Rols, M.-P., Cemazar, M., and Golzio, M. (2016) Visualization of nonspecific antitumor effectiveness and vascular effects of gene electro-transfer to tumors, *Curr. Gene Ther.*, **16**, 90-97.
69. Krumholz, A., Shcherbakova, D. M., Xia, J., Wang, L. V., and Verkhusha, V. V. (2014) Multicontrast photoacoustic *in vivo* imaging using near-infrared fluorescent proteins, *Sci. Rep.*, **4**, 3939.
70. Lai, C.-W., Chen, H.-L., Yen, C.-C., Wang, J.-L., Yang, S.-H., and Chen, C.-M. (2016) Using dual fluorescence reporting genes to establish an *in vivo* imaging model of orthotopic lung adenocarcinoma in mice, *Mol. Imaging Biol.*, **18**, 849-859.
71. Lu, Y., Darne, C. D., Tan, I.-C., Wu, G., Wilganowski, N., Robinson, H., Azhdarinia, A., Zhu, B., Rasmussen, J. C., and Sevick-Muraca, E. M. (2013) *In vivo* imaging of orthotopic prostate cancer with far-red gene reporter fluorescence tomography and *in vivo* and *ex vivo* validation, *J. Biomed. Opt.*, **18**, 101305.
72. Nedosekin, D. A., Sarimollaoglu, M., Galanzha, E. I., Sawant, R., Torchilin, V. P., Verkhusha, V. V., Ma, J., Frank, M. H., Biris, A. S., and Zharov, V. P. (2013) Synergy of photoacoustic and fluorescence flow cytometry of circulating cells with negative and positive contrasts, *J. Biophotonics*, **6**, 425-434.
73. Oliveira, J. C., da Silva, A. C., Oliveira, R. A. D. S., Pereira, V. R. A., and Gil, L. H. V. G. (2016) *In vivo* near-infrared fluorescence imaging of *Leishmania amazonensis* expressing infrared fluorescence protein (iRFP) for real-time monitoring of *Cutaneous leishmaniasis* in mice, *J. Microbiol. Meth.*, **130**, 189-195.
74. Paulus-Hock, V., Cheung, E. C., Roxburgh, P., Vousden, K. H., and Hock, A. K. (2014) iRFP is a real time marker for transformation-based assays in high content screening, *PLoS One*, **9**, e98399.
75. Richie, C. T., Whitaker, L. R., Whitaker, K. W., Necarsulmer, J., Baldwin, H. A., Zhang, Y., Fortuno, L., Hinkle, J. J., Koivula, P., Henderson, M. J., Sun, W., Wang, K., Smith, J. C., Pickel, J., Ji, N., Hope, B. T., and Harvey, B. K. (2017) Near-infrared fluorescent protein iRFP713 as a reporter protein for optogenetic vectors, a transgenic cre-reporter rat, and other neuronal studies, *J. Neurosci. Meth.*, **284**, 1-14.
76. Roman, W., Martins, J. P., Carvalho, F. A., Voituriez, R., Abella, J. V. G., Santos, N. C., Cadot, B., Way, M., and Gomes, E. R. (2017) Myofibril contraction and crosslinking drive nuclear movement to the periphery of skeletal muscle, *Nat. Cell Biol.*, **19**, 1189-1201.
77. Spronken, M. I., Short, K. R., Herfst, S., Bestebroer, T. M., Vaes, V. P., van der Hoeven, B., Koster, A. J., Kremers, G.-J., Scott, D. P., Gultyaev, A. P., Sorell, E. M., de Graaf, M., Barcena, M., Rimmelzwaan, G. F., and Fouchier, R. A. (2015) Optimizations and challenges involved in the creation of various bioluminescent and fluorescent influenza A virus strains for *in vitro* and *in vivo* applications, *PLoS One*, **10**, e0133888.
78. Stabley, D. R., Oh, T., Simon, S. M., Mattheyses, A. L., and Salaita, K. (2015) Real-time fluorescence imaging with 20 nm axial resolution, *Nat. Commun.*, **6**, 8307.
79. Tanaka, N., Lajud, S. A., Ramsey, A., Szymanowski, A. R., Ruffner, R., O'Malley, B. W., and Li, D. (2016) Application of infrared-based molecular imaging to a mouse model with head and neck cancer, *Head Neck*, **38** (Suppl. 1), E1351-E1357.
80. Tzoumas, S., Nunes, A., Deliolanis, N. C., and Ntziachristos, V. (2015) Effects of multispectral excitation on the sensitivity of molecular optoacoustic imaging, *J. Biophotonics*, **8**, 629-637.
81. Wang, K., Sun, W., Richie, C. T., Harvey, B. K., Betzig, E., and Ji, N. (2015) Direct wavefront sensing for high-resolution *in vivo* imaging in scattering tissue, *Nat. Commun.*, **6**, 7276.
82. Zhu, B., Wu, G., Robinson, H., Wilganowski, N., Hall, M. A., Ghosh, S. C., Pinkston, K. L., Azhdarinia, A., Harvey, B. R., and Sevick-Muraca, E. M. (2013) Tumor margin detection using quantitative NIRF molecular imaging targeting EpCAM validated by far red gene reporter iRFP, *Mol. Imag. Biol.*, **15**, 560-568.
83. Zhu, B., Robinson, H., Zhang, S., Wu, G., and Sevick-Muraca, E. M. (2015) Longitudinal far red gene-reporter imaging of cancer metastasis in preclinical models: a tool for accelerating drug discovery, *Biomed. Opt. Express*, **6**, 3346-3351.
84. To, T.-L., Piggott, B. J., Makhijani, K., Yu, D., Jan, Y. N., and Shu, X. (2015) Rationally designed fluorogenic protease reporter visualizes spatiotemporal dynamics of apoptosis *in vivo*, *Proc. Natl. Acad. Sci. USA*, **112**, 3338-3343.
85. Donnelly, S. K., Cabrera, R., Mao, S. P. H., Christin, J. R., Wu, B., Guo, W., Bravo-Cordero, J. J., Condeelis, J. S., Segall, J. E., and Hodgson, L. (2017) Rac3 regulates breast cancer invasion and metastasis by controlling adhesion and matrix degradation, *J. Cell Biol.*, **216**, 4331-4349.
86. Kyung, T., Lee, S., Kim, J. E., Cho, T., Park, H., Jeong, Y.-M., Kim, D., Shin, A., Kim, S., Baek, J., Kim, J., Kim, N. Y., Woo, D., Chae, S., Kim, C.-H., Shin, H.-S., Han, Y.-M., Kim, D., and Heo, W. D. (2015) Optogenetic control of endogenous Ca^{2+} channels *in vivo*, *Nat. Biotechnol.*, **33**, 1092-1096.
87. Piatkevich, K. D., Suk, H.-J., Kodandaramaiah, S. B., Yoshida, F., DeGennaro, E. M., Drobizhev, M., Hughes, T. E., Desimone, R., Boyden, E. S., and Verkhusha, V. V. (2017) Near-infrared fluorescent proteins engineered from bacterial phytochromes in neuroimaging, *Biophys. J.*, **113**, 2299-2309.
88. Fyk-Kolodziej, B., Hellmer, C. B., and Ichinose, T. (2014) Marking cells with infrared fluorescent proteins to preserve photoresponsiveness in the retina, *BioTechniques*, **57**, 245-253.
89. Satoh, T., Baba, M., Nakatsuka, D., Ishikawa, Y., Aburatani, H., Furuta, K., Ishikawa, T., Hatanaka, H., Suzuki, M., and Watanabe, Y. (2003) Role of heme oxygenase-1 protein in the neuroprotective effects of cyclopentenone prostaglandin derivatives under oxidative stress, *Eur. J. Neurosci.*, **17**, 2249-2255.
90. Gibbs, P. E. M., and Maines, M. D. (2007) Biliverdin inhibits activation of NF-kappaB: reversal of inhibition by human biliverdin reductase, *Int. J. Cancer*, **121**, 2567-2574.

91. Miralem, T., Lerner-Marmarosh, N., Gibbs, P. E. M., Tudor, C., Hagen, F. K., and Maines, M. D. (2012) The human biliverdin reductase-based peptide fragments and biliverdin regulate protein kinase Cδ activity, *J. Biol. Chem.*, **287**, 24698-24712.
92. Molzer, C., Pfleger, B., Putz, E., RoЯmann, A., Schwarz, U., Wallner, M., Bulmer, A. C., and Wagner, K.-H. (2013) *In vitro* DNA-damaging effects of intestinal and related tetrapyrroles in human cancer cells, *Exp. Cell Res.*, **319**, 536-545.
93. Nuhn, P., Kunzli, B. M., Hennig, R., Mitkus, T., Ramanauskas, T., Nobiling, R., Meuer, S. C., Friess, H., and Berberat, P. O. (2009) Heme oxygenase-1 and its metabolites affect pancreatic tumor growth *in vivo*, *Mol. Cancer*, **8**, 37.
94. Chen, K., Gunter, K., and Maines, M. D. (2000) Neurons overexpressing heme oxygenase-1 resist oxidative stress-mediated cell death, *J. Neurochem.*, **75**, 304-313.
95. Song, W., Su, H., Song, S., Paudel, H. K., and Schipper, H. M. (2006) Over-expression of heme oxygenase-1 promotes oxidative mitochondrial damage in rat astroglia, *J. Cell. Physiol.*, **206**, 655-663.
96. Takeda, A., Perry, G., Abraham, N. G., Dwyer, B. E., Kutty, R. K., Laitinen, J. T., Petersen, R. B., and Smith, M. A. (2000) Overexpression of heme oxygenase in neuronal cells, the possible interaction with tau, *J. Biol. Chem.*, **275**, 5395-5399.
97. Honda, M., Yogosawa, S., Kamada, M., Kamata, Y., Kimura, T., Koike, Y., Harada, T., Takahashi, H., Egawa, S., and Yoshida, K. (2017) A novel near-infrared fluorescent protein, iRFP720, facilitates transcriptional profiling of prostate cancer bone metastasis in mice, *Anticancer Res.*, **37**, 3009-3013.
98. Huang, C., Lan, W., Wang, F., Zhang, C., Liu, X., and Chen, Q. (2017) AAV-iRFP labelling of human mesenchymal stem cells for near-infrared fluorescence imaging, *Biosci. Rep.*, **37**, BSR20160556.
99. Sita, T. L., Kouri, F. M., Hurley, L. A., Merkel, T. J., Chalastanis, A., May, J. L., Ghelfi, S. T., Cole, L. E., Cayton, T. C., Barnaby, S. N., Sprangers, A. J., Savalia, N., James, C. D., Lee, A., Mirkin, C. A., and Stegh, A. H. (2017) Dual bioluminescence and near-infrared fluorescence monitoring to evaluate spherical nucleic acid nanoconjugate activity *in vivo*, *Proc. Natl. Acad. Sci. USA*, **114**, 4129-4134.
100. Rumyantsev, K. A., Turoverov, K. K., and Verkhusha, V. V. (2016) Near-infrared bioluminescent proteins for two-color multimodal imaging, *Sci. Rep.*, **6**, 36588.
101. Mezzanotte, L., Iljas, J. D., Que, I., Chan, A., Kaijzel, E., Hoeben, R., and Lowik, C. (2017) Optimized longitudinal monitoring of stem cell grafts in mouse brain using a novel bioluminescent/near infrared fluorescent fusion reporter, *Cell Transplant.*, **26**, 1878-1889.
102. Isomura, M., Yamada, K., Noguchi, K., and Nishizono, A. (2017) Near-infrared fluorescent protein iRFP720 is optimal for *in vivo* fluorescence imaging of rabies virus infection, *J. Gen. Virol.*, **98**, 2689-2698.
103. Telford, W. G., Shcherbakova, D. M., Buschke, D., Hawley, T. S., and Verkhusha, V. V. (2015) Multiparametric flow cytometry using near-infrared fluorescent proteins engineered from bacterial phytochromes, *PLoS One*, **10**, e0122342.
104. Zhang, X.-E., Cui, Z., and Wang, D. (2016) Sensing of biomolecular interactions using fluorescence complementing systems in living cells, *Biosens. Bioelectron.*, **76**, 243-250.
105. Kodama, Y., and Hu, C.-D. (2012) Bimolecular fluorescence complementation (BiFC): a 5-year update and future perspectives, *BioTechniques*, **53**, 285-298.
106. Miller, K. E., Kim, Y., Huh, W.-K., and Park, H.-O. (2015) Bimolecular fluorescence complementation (BiFC) analysis: advances and recent applications for genome-wide interaction studies, *J. Mol. Biol.*, **427**, 2039-2055.
107. Hirata, E., and Kiyokawa, E. (2016) Future perspective of single-molecule FRET biosensors and intravital FRET microscopy, *Biophys. J.*, **111**, 1103-1111.
108. Hochreiter, B., Pardo-Garcia, A., and Schmid, J. A. (2015) Fluorescent proteins as genetically encoded FRET biosensors in life sciences, *Sensors*, **15**, 26281-26314.
109. Komatsu, N., Aoki, K., Yamada, M., Yukinaga, H., Fujita, Y., Kamioka, Y., and Matsuda, M. (2011) Development of an optimized backbone of FRET biosensors for kinases and GTPases, *Mol. Biol. Cell*, **22**, 4647-4656.
110. Chen, M., Li, W., Zhang, Z., Liu, S., Zhang, X., Zhang, X.-E., and Cui, Z. (2015) Novel near-infrared BiFC systems from a bacterial phytochrome for imaging protein interactions and drug evaluation under physiological conditions, *Biomaterials*, **48**, 97-107.
111. Li, L., Shemetov, A. A., Baloban, M., Hu, P., Zhu, L., Shcherbakova, D. M., Zhang, R., Shi, J., Yao, J., Wang, L. V., and Verkhusha, V. V. (2018) Small near-infrared photochromic protein for photoacoustic multi-contrast imaging and detection of protein interactions *in vivo*, *Nat. Commun.*, **9**, 2734.
112. Zlobovskaya, O. A., Sergeeva, T. F., Shirmanova, M. V., Dudenkova, V. V., Sharonov, G. V., Zagaynova, E. V., and Lukyanov, K. A. (2016) Genetically encoded far-red fluorescent sensors for caspase-3 activity, *BioTechniques*, **60**, 62-68.
113. Sakaue-Sawano, A., Kurokawa, H., Morimura, T., Hanyu, A., Hama, H., Osawa, H., Kashiwagi, S., Fukami, K., Miyata, T., Miyoshi, H., Imamura, T., Ogawa, M., Masai, H., and Miyawaki, A. (2008) Visualizing spatiotemporal dynamics of multicellular cell-cycle progression, *Cell*, **132**, 487-498.
114. Chudakov, D. M., Matz, M. V., Lukyanov, S., and Lukyanov, K. A. (2010) Fluorescent proteins and their applications in imaging living cells and tissues, *Physiol. Rev.*, **90**, 1103-1163.
115. Stuker, F., Ripoll, J., and Rudin, M. (2011) Fluorescence molecular tomography: principles and potential for pharmaceutical research, *Pharmaceutics*, **3**, 229-274.
116. Zanca, C., Villa, G. R., Benitez, J. A., Thorne, A. H., Koga, T., D'Antonio, M., Ikegami, S., Ma, J., Boyer, A. D., Banisadr, A., Jameson, N. M., Parisian, A. D., Eliseeva, O. V., Barnabe, G. F., Liu, F., Wu, S., Yang, H., Wykosky, J., Frazer, K. A., Verkhusha, V. V., Isaguliants, M. G., Weiss, W. A., Gahman, T. C., Shiau, A. K., Chen, C. C., Mischel, P. S., Cavenee, W. K., and Furnari, F. B. (2017) Glioblastoma cellular cross-talk converges on NF-kB to attenuate EGFR inhibitor sensitivity, *Genes Dev.*, **31**, 1212-1227.
117. Rice, W. L., Shcherbakova, D. M., Verkhusha, V. V., and Kumar, A. T. N. (2015) *In vivo* tomographic imaging of

deep-seated cancer using fluorescence lifetime contrast, *Cancer Res.*, **75**, 1236-1243.
118. Wang, L. V., and Hu, S. (2012) Photoacoustic tomography: *in vivo* imaging from organelles to organs, *Science*, **335**, 1458-1462.
119. Chan, X. H. D., Balasundaram, G., Attia, A. B. E., Goggi, J. L., Ramasamy, B., Han, W., Olivo, M., and Sugii, S. (2018) Multimodal imaging approach to monitor browning of adipose tissue *in vivo*, *J. Lipid Res.*, **59**, 1071-1078.
120. Yao, J., Kaberniuk, A. A., Li, L., Shcherbakova, D. M., Zhang, R., Wang, L., Li, G., Verkhusha, V. V., and Wang, L. V. (2016) Multiscale photoacoustic tomography using reversibly switchable bacterial phytochrome as a near-infrared photochromic probe, *Nat. Methods*, **13**, 67-73.
121. Dortay, H., Mark, J., Wagener, A., Zhang, E., Grotzinger, C., Hildebrandt, P., Friedrich, T., and Laufer, J. (2016) Dual-wavelength photoacoustic imaging of a photoswitchable reporter protein, in *Photons Plus Ultrasound: Imaging and Sensing 2016*, International Society for Optics and Photonics, 970820.
122. Mark, J., Dortay, H., Wagener, A., Zhang, E., Buchmann, J., Grotzinger, C., Friedrich, T., and Laufer, J. (2018) Dual-wavelength 3D photoacoustic imaging of mammalian cells using a photoswitchable phytochrome reporter protein, *Commun. Phys.*, **1**, 3.
123. Van Veen, R. L., Sterenborg, H. J., Pifferi, A., Torricelli, A., and Cubeddu, R. (2005) Determination of VIS-NIR absorption coefficients of mammalian fat, with time- and spatially resolved diffuse reflectance and transmission spectroscopy, *J. Biomed. Optics*, **10**, 054004.
124. Palmer, K. F., and Williams, D. (1974) Optical properties of water in the near infrared, *JOSA*, **64**, 1107-1110.
125. Buiteveld, H., Hakvoort, J. H. M., and Donze, M. (1994) Optical properties of pure water, *SPIE*, **2258**, 174-184.
126. Otero, L. H., Klinke, S., Rinaldi, J., Velazquez-Escobar, F., Mroginski, M. A., Fernandez Lopez, M., Malamud, F., Vojnov, A. A., Hildebrandt, P., Goldbaum, F. A., and Bonomi, H. R. (2016) Structure of the full-length bacteriophytochrome from the plant pathogen *Xanthomonas campestris* provides clues to its long-range signaling mechanism, *J. Mol. Biol.*, **428**, 3702-3720.